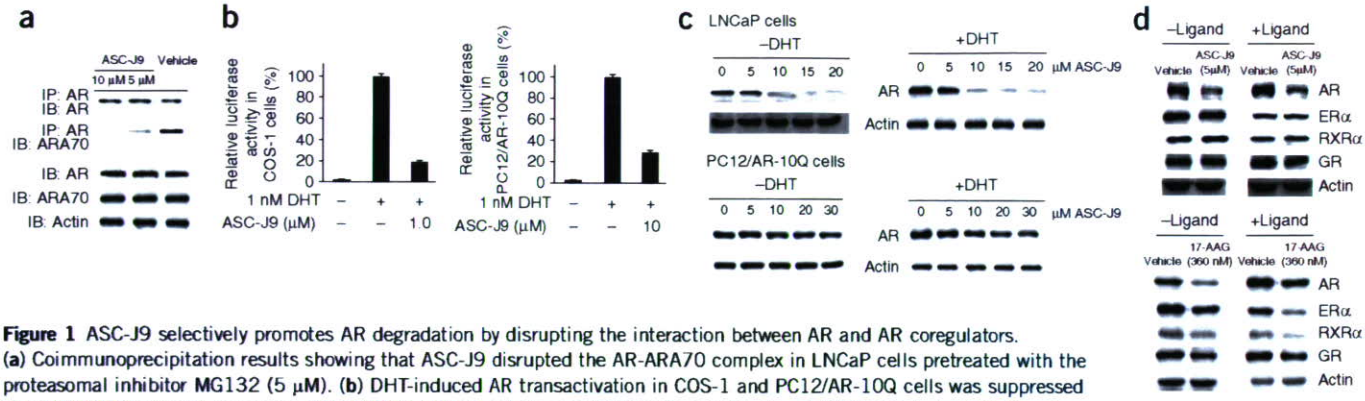

Figure 1 ASC-J9 selectively promotes AR degradation by disrupting the interaction between AR and AR coregulators. (**a**) Coimmunoprecipitation results showing that ASC-J9 disrupted the AR-ARA70 complex in LNCaP cells pretreated with the proteasomal inhibitor MG132 (5 μM). (**b**) DHT-induced AR transactivation in COS-1 and PC12/AR-10Q cells was suppressed after ASC-J9 treatment, as assessed by (ARE)4-LUC reporter assay. (**c**) The steady-state level of AR protein in LNCaP and PC12/AR-10Q cells from western blot assays indicated that the AR signal decreased substantially (in a dose-dependent manner) after treatment with ASC-J9. (**d**) ASC-J9 selectively decreased the steady-state level of AR protein, in the absence and the presence of ligand. In contrast, 17-AAG treatment decreased the steady-state level of all four ligand-activated nuclear receptors (AR, ERα, GR and RXRα), both in the absence and in the presence of the specific ligand.

Moreover, the SBMA mice showed normal sexual activity and improved fertility, suggesting that this strategy might provide a better approach to treating SBMA in men.

RESULTS

ASC-J9 selectively promotes AR degradation

To test our hypothesis that disrupting the interaction between AR and AR-associated proteins is an improved strategy for battling SBMA, we first used a coimmunoprecipitation assay in cultured prostate cancer LNCaP cells, which demonstrated that ASC-J9 promotes the dissociation between AR and its coregulator ARA70 (**Fig. 1a**). We then found that, in COS-1 cells, ASC-J9–induced dissociation between AR and ARA70 led to suppression of AR transactivation (**Fig. 1b**). Similar suppression effects also occurred when we replaced COS-1 cells with PC12/AR-10Q cells (**Fig. 1b**).

To determine whether AR degrades more rapidly when freed of its association with coregulators, we measured the steady-state level of AR protein after the administration of different doses of ASC-J9 in LNCaP and PC12/AR-10Q cells. ASC-J9 treatment decreased the steady-state level of AR protein in the absence and presence of the hormone dihydrotestosterone (DHT), suggesting that ASC-J9 might promote AR protein degradation by disrupting the interaction of AR with AR coregulators (**Fig. 1c**). As the interaction between AR and ARA70 is relatively selective[9], we expected that the degradation of AR by ASC-J9 would also be selective. Whereas ASC-J9 promoted the degradation of AR, it had little effect on other members of the family of ligand-activated nuclear receptors, such as glucocorticoid receptor (GR), estrogen receptor-α (ERα) and retinoid X receptor-α RXRα (**Fig. 1d**). In contrast, the hsp90 inhibitor 17-allylamino-17-demethoxygeldanamycin (17-AAG), which uncouples the interaction between hsp90 and members of this family, unselectively promoted the degradation of AR as well as GR, ERα and RXRα.

Collectively, the results demonstrated that ASC-J9, but not 17-AAG, classic antiandrogen hydroxyflutamide (HF) or curcumin (**Fig. 1d** and **Supplementary Fig. 1** online), can selectively promote AR degradation, which might be secondary to disrupting the interaction between AR and AR coregulators, which results in the suppression of AR transactivation.

ASC-J9 reduces the AR aggregated AR-112Q in cells

The aggregation of AR-polyQ in the nucleus, which is toxic to motor neurons, has been linked to the pathogenesis of SBMA (ref. 11). We tested PC12 cells stably transfected with inducible AR-112Q (PC12/AR-112Q) in a model that mimics the nuclear aggregation present in SBMA (ref. 23) to see whether ASC-J9 can reduce the pathogenesis of SBMA. We found that AR-112Q localized in the cytoplasm in the

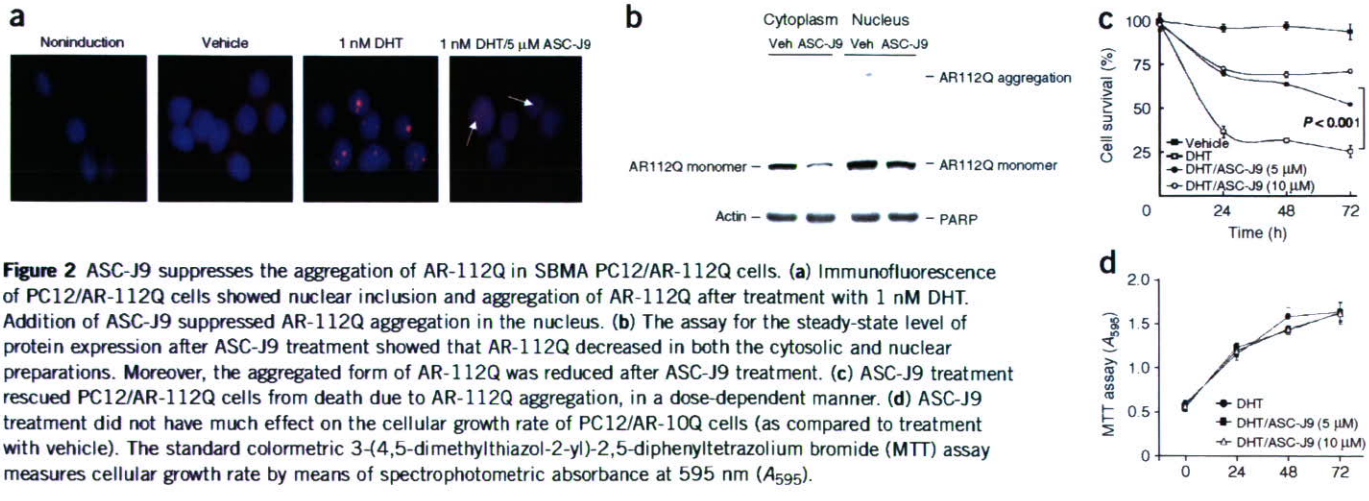

Figure 2 ASC-J9 suppresses the aggregation of AR-112Q in SBMA PC12/AR-112Q cells. (**a**) Immunofluorescence of PC12/AR-112Q cells showed nuclear inclusion and aggregation of AR-112Q after treatment with 1 nM DHT. Addition of ASC-J9 suppressed AR-112Q aggregation in the nucleus. (**b**) The assay for the steady-state level of protein expression after ASC-J9 treatment showed that AR-112Q decreased in both the cytosolic and nuclear preparations. Moreover, the aggregated form of AR-112Q was reduced after ASC-J9 treatment. (**c**) ASC-J9 treatment rescued PC12/AR-112Q cells from death due to AR-112Q aggregation, in a dose-dependent manner. (**d**) ASC-J9 treatment did not have much effect on the cellular growth rate of PC12/AR-10Q cells (as compared to treatment with vehicle). The standard colormetric 3-(4,5-dimethylthiazol-2-yl)-2,5-diphenyltetrazolium bromide (MTT) assay measures cellular growth rate by means of spectrophotometric absorbance at 595 nm (A_{595}).

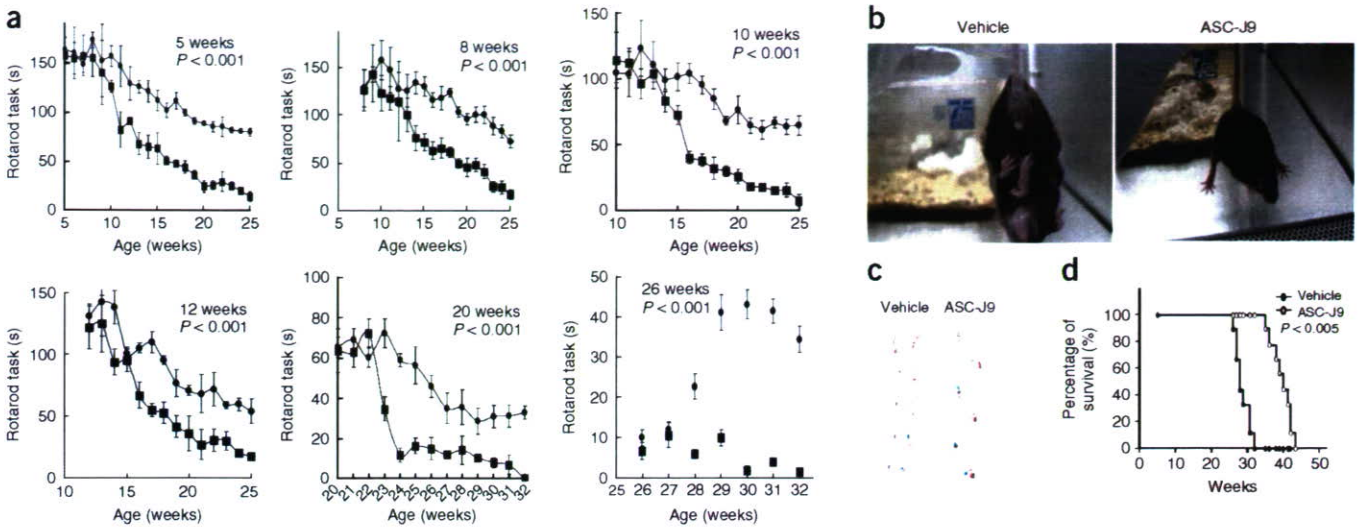

Figure 3 Effects of ASC-J9 (50 mg/kg every 48 h) on SBMA symptoms in male SBMA mice. (**a**) Performance of mice of different ages on the rotarod tasks ($n = 6$ in each group). Mice treated with ASC-J9 showed noticeable improvement even when the treatment started as late as 26 weeks after the onset of SBMA phenotype. (**b–d**) SBMA mice were treated with vehicle or ASC-J9 starting at 5 weeks, and were examined at 15 weeks. With ASC-J9, phenotypic clasping behavior was ameliorated (**b**), footprint patterns were normal (**c**) and the survival rate had improved (**d**) ($n = 9$ mice in each group). In **c**, front paws are in blue and hind paws in red.

absence of DHT, and addition of 1 nM DHT resulted in the translocation of AR-112Q into the nucleus and subsequent formation of aggregates (**Fig. 2a**). Notably, addition of 5 μM ASC-J9 substantially suppressed the aggregate formation, with little AR-112Q detected in the nucleus (**Fig. 2a**). Western blotting analysis also showed that ASC-J9 treatment promoted the degradation and reduced the amount of aggregated AR-112Q protein in the nucleus (**Fig. 2b**).

In addition, PC12 cell death induced by AR-112Q nuclear aggregation was rescued by the addition of ASC-J9 in a dose-dependent manner (**Fig. 2c**), with little influence on the proliferation of PC12/AR-10Q cells (**Fig. 2d**). Collectively, these results demonstrated that ASC-J9 might reduce cytotoxicity by suppressing the aggregation of AR-112Q in the nucleus and increasing its degradation in the PC12/AR-112Q cells, with little effect on the PC12/AR-10Q cells.

ASC-J9 rescues the SBMA symptoms in AR-97Q mice

We further examined the *in vivo* effects of ASC-J9 in SBMA mice with transgenic AR-97Q (ref. 5). Every other day, we injected male SBMA mice intraperitoneally with ASC-J9 in corn oil at the effective dose of 50 mg per kg body weight, and assessed their motor impairment by testing rotarod activity weekly. We found that the motor impairments were substantially improved in SBMA mice treated with ASC-J9, regardless of whether treatment was started early (at 5 weeks of age) or later (at 26 weeks) (**Fig. 3a**). This observation suggests that ASC-J9 treatment substantially delays the onset and symptomatic progression of motor impairment, which usually appears at 10 weeks. We also found that cage activity increased in SBMA mice treated with ASC-J9 (**Supplementary Video 1** online). The SBMA symptoms of gait disturbance, including severe dragging of hind limbs and erratic footprinting patterns, markedly declined in ASC-J9–treated SBMA mice, suggesting that ASC-J9 treatment can substantially ameliorate the SBMA symptoms in these mice (**Fig. 3b,c**). Notably, ASC-J9 treatment prolonged the lives of these mice, from an average of 28 weeks to 39 weeks (**Fig. 3d**).

Improved sexual functions in SBMA mice treated with ASC-J9

SBMA patients might be reluctant to undergo the helpful but aggressive treatment of surgical or chemical castration because such treatments suppress serum testosterone levels, leading to a loss of normal sexual genital functions and fertility. Notably, we found that ASC-J9–treated SBMA mice had relatively normal serum testosterone concentrations (**Fig. 4a**). Sexual activity, as judged by vaginal plug numbers in female mice caged with the treated males, and fertility, as judged by both pup numbers and litter numbers, were substantially improved during 4 weeks of fertility tests (**Fig. 4b**).

These results demonstrated that there was little adverse influence on serum testosterone and that sexual genital functions and fertility were in fact improved in SBMA mice treated with ASC-J9.

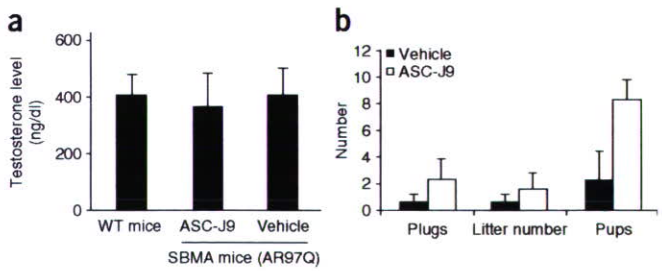

Figure 4 Effect of ASC-J9 (50 mg/kg every 48h) on the fertility and testosterone level of male SBMA mice. We began treatment of SBMA mice at 5 weeks of age. (**a**) We took blood samples from wild-type (WT) and vehicle- or ASC-J9–treated SBMA mice at 20 weeks of age ($n = 9$ mice in each group), and measured serum testosterone levels using an ELISA kit. We found little difference between vehicle- and ASC-J9–treated mice in terms of serum testosterone levels. (**b**) Fertility tests performed on 13-week-old SBMA mice ($n = 4$ mice in each group) showed increased sexual activity following ASC-J9 treatment (compared to vehicle treatment).

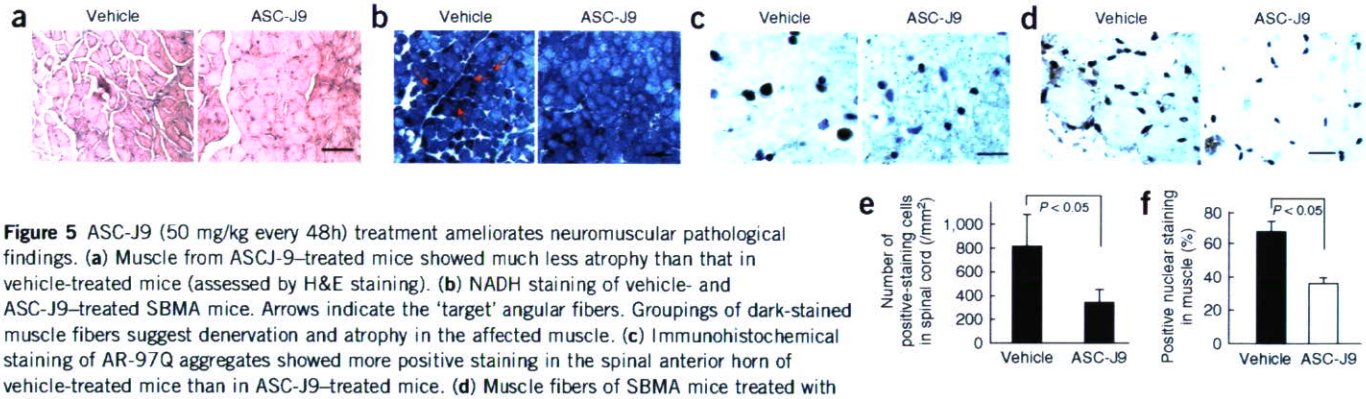

Figure 5 ASC-J9 (50 mg/kg every 48h) treatment ameliorates neuromuscular pathological findings. (**a**) Muscle from ASCJ-9–treated mice showed much less atrophy than that in vehicle-treated mice (assessed by H&E staining). (**b**) NADH staining of vehicle- and ASC-J9–treated SBMA mice. Arrows indicate the 'target' angular fibers. Groupings of dark-stained muscle fibers suggest denervation and atrophy in the affected muscle. (**c**) Immunohistochemical staining of AR-97Q aggregates showed more positive staining in the spinal anterior horn of vehicle-treated mice than in ASC-J9–treated mice. (**d**) Muscle fibers of SBMA mice treated with ASC-J9 showed much less aggregation of AR-112Q than the muscle fibers from vehicle-treated SBMA mice. (**e**,**f**) There was approximately 50% reduction in AR-aggregated positive-staining cells in the spinal cord and the muscle fibers after ASC-J9 treatment compared with vehicle treatment. Scale bars: 100 μm in **a** and **b**, 20 μm in **c** and **d**.

ASC-J9 reverses muscular atrophy and restores VEGF expression

Hematoxylin and eosin staining showed that ASC-J9 treatment substantially reduced muscular atrophy compared to vehicle treatment (**Fig. 5a**). By using nicotinamide adenine dinucleotide (NADH) to stain muscle, we also found that the groupings of muscle fibers were markedly altered in the ASC-J9–treated mice (**Fig. 5b**). There were more groupings of ankylated muscle fibers, suggesting the denervation and atrophy of muscle fibers, in vehicle-treated mice than in ASC-J9–treated mice (**Fig. 5b**). Immunohistochemical staining using an antibody to AR, N20, showed the intranuclear aggregation of AR-97Q in spinal cord motor neurons and skeletal muscle cells (**Fig. 5c,d**). Also, the intranuclear AR-97Q aggregation in spinal cord neurons and muscle cells was significantly lower (by almost 50%) in the ASC-J9–treated mice than in the vehicle-treated mice (**Fig. 5e,f**).

Motor neuron survival and proper function requires VEGF164 expression. Previous studies have suggested that aggregated AR-97Q might associate abnormally with CBP, resulting in the disruption of CBP-mediated VEGF164 expression[24]. By examining coimmunoprecipitation in PC12/AR-112Q and PC12/AR-Q10 cells, we found that ASC-J9 dose-dependently disrupted the interaction between AR-112Q and CBP in PC12/AR-112Q cells but had little influence in PC12/AR-10Q cells (**Fig. 6a**). Releasing CBP from its interaction with AR-112Q in PC12/AR-112Q cells was associated with the induction of VEGF164 expression (**Fig. 6b**).

We further confirmed this finding by showing a significant increase (from 20% to 90%) in the expression of mRNA for VEGF164 in the spinal cord of SBMA mice following ASC-J9 treatment (**Fig. 6c**). Moreover, the ELISA assay to detect the levels of VEGF protein in the spinal cord of these mice also demonstrated a significant increase of VEGF expression after ASC-J9 treatment (**Fig. 6d**). These results do not formally prove that ASC-J9 ameliorates SBMA symptoms by restoring VEGF164 expression, but they are consistent with this idea.

DISCUSSION

It has been shown that one of hsp90's associated proteins, AR, can be degraded when the interaction between hsp90 and its associated proteins is disrupted by using the hsp90 inhibitor 17-AAG. This degradation reduces the longer AR-97Q nuclear aggregates in SBMA mice[25]. However, 17-AAG also disrupts the interaction between hsp90 and many other proteins, including GR, ERα and RXRα (**Fig. 1d**), and Her2, Her3 receptor tyrosine kinase, Erk1/2 and Rb (refs. 25–30), rendering them more susceptible to degradation. Recent reports have clearly documented that common adverse reactions to 17-AAG include anorexia, diarrhea, nausea, fatigue and vomiting, along with the reversible elevation of liver enzymes (in 29.5% of subjects)[31]. This inhibitor also enhances bone metastasis and osteolytic lesions, which

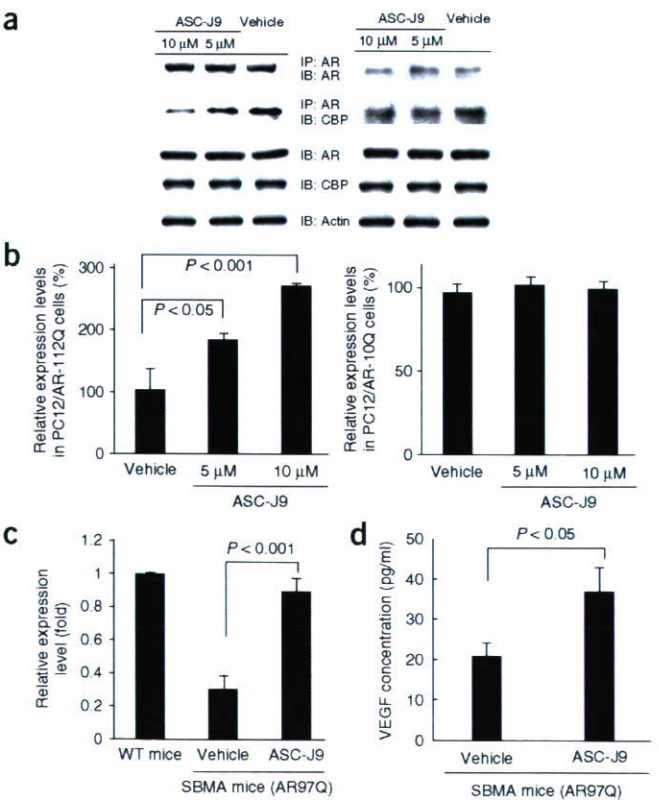

Figure 6 Molecular mechanisms of the effect of ASC-J9 on the SBMA phenotypes. (**a**) Treatment with 5 μM or 10 μM ASC-J9 showed dose-dependent disruption of the interaction between CBP and AR-112Q or AR-10Q in PC12 cells pretreated with the proteasomal inhibitor MG132 (5 μM). (**b**) ASC-J9 treatment increased VEGF164 expression in PC12/AR-112Q cells but had little influence in PC12/AR-10Q cells pretreated with MG132. (**c**) ASC-J9 treatment had a dose-dependent effect on increasing mRNA for VEGF164 in the spinal cord. (**d**) Amounts of VEGF protein from homogenized L5 spinal cords were increased after ASC-J9 treatment.

lead to increased osteolysis and incidence of skeletal tumors[32]. The nonspecific disruption by 17-AAG of the interaction between hsp90 and most of its associated proteins leads to extensive adverse and unwanted side effects, and therefore limits the applicability of 17-AAG in the treatment of SBMA. In contrast, ASC-J9 (at a dose of 50 mg/kg every 48 h for more than 20 weeks) had no obvious toxic effects and did not result in a loss of body weight in mice. Moreover, the sexual genital functions and fertility in these SBMA mice were improved markedly. Together, these positive results of ASC-J9 treatment demonstrate that this new approach—involving the selective disruption of interactions between AR-polyQ and AR coregulators, such as CBP—might offer improved treatment for SBMA. Additional dosage studies of ASC-J9 or its derivatives to investigate how SBMA symptoms may be effectively ameliorated, without toxicity, might lead to treatments that could substantially improve the quality of life of SBMA patients.

METHODS

Therapeutic agent and administration protocol. ASC-J9 from AndroScience was synthesized as described previously[22]. We dissolved it in corn oil and injected it intraperitoneally into mice (50 mg/kg every other day) at various ages until the end of the study. Control mice received DMSO in corn oil only.

ASC-J9 characterization. For the AR degradation study, we treated LNCaP cells with vehicle and 1 nM DHT with or without 5 μM ASC-J9, in RPMI supplemented with 10% charcoal dextran–stripped (CDS) FBS. At selected time intervals, we harvested cells and analyzed AR protein levels by western blotting, quantitated the results by Bio-Rad PDQuest Image software, and normalized densitometric values to actin. We purchased the antibodies for AR (N20), CBP (C-1), ERα (HC-20), GR (P-20), RXRα (D-20), CBP, PARP and actin from Santa Cruz Biotechnology and generated ARA70 antibody as previously described[33].

For the AR-112Q protein steady-state assay, we cultured PC12/AR-112Q cells as described previously[23], in the presence of 10 μg/ml doxycycline for 24 h, and then treated cells with or without 1 nM DHT or 1 nM DHT and 5 μM ASC-J9 for 3 d. We performed the cytosolic and nuclear extraction by FractionPREP™ Cell Fraction System (BioVision) and analyzed the AR-112Q by western blotting.

We performed the protein steady-state assay of AR, GR, ERα and RXRα in response to 5 μM ASC-J9 or 360 nM 17-AAG, on LNCaP cells (AR and RXRα), MCF-7 cells (ERα) and PC3 cells (GR), in the presence or absence of ligand (1 nM DHT for AR, 1 nM E2 for ERα, 1 nM dexamethasone for GR and 1 μM 9-cis-RA for RXRα). We determined the amounts of AR, GR, ERα and RXRα proteins by western blotting and analyzed the interactions between AR-ARA70 complex and AR-CBP complex by coimmunoprecipitation[24,33]. We assayed AR transactivation activity as described previously[34].

Immunofluorescence staining and cell survival. We cultured PC12/AR-112Q cells in two-well Chamber slides (Nalge Nunc) supplemented by DMEM, 10% CDS horse serum and 100 μg/ml nerve growth factor (BD Biosciences), and induced AR-112Q by 10 μg/ml doxycycline (Sigma) for 4 h. Then we treated cells with vehicle, 1 nM DHT, or 1 nm DHT and 5 μM ASC-J9 for 3 d. We stained AR-112Q with N20 antibody and Texas Red–conjugated streptavidin (Vector Laboratories), mounted slides in fluorescent mounting medium containing 4′,6-diamidino-2-phenylindole (DAPI), and observed fluorescent staining using an Olympus fluorescent microscope.

For the cell survival assay, we cultured PC12/AR-112Q and PC12/AR-10Q cells as described previously[23] and incubated cells in the presence of 10 μg/ml doxycycline for 24 h. Then we treated cells with vehicle, 5 μM ASC-J9 or 10 μM ASC-J9, along with 1 nM DHT, and determined cell viability using Trypan blue staining at specific time intervals.

SBMA mouse model generation, maintenance, genotyping and motor activity assessment. We generated the AR-97Q SBMA mice as described previously[5]. We performed all animal experiments in accordance with the Guide for the Care and Use of Laboratory Animals of the US National Institutes of Health and with approval from the Department of Laboratory Animal Medicine at the University of Rochester. We assessed rotarod performance weekly using an Economex Rotarod (Colombus Instruments) as described[35], and observed footprints for ASC-J9– or vehicle-treated SBMA mice by dipping their forepaws in water-soluble red paint and hind paws in blue paint. The mice then walked through a narrow tunnel, leaving footprints on a strip of white paper[21].

Serum testosterone and male fertility. We killed SBMA mice receiving ASC-J9 or vehicle treatment at 20 weeks of age, drew 1 ml of blood by cardiocentesis, and assayed serum testosterone with the Coat-A-Count Total Testosterone radioimmunoassay (Diagnostic Products) according to the manufacturer's protocol. We observed the reproductive capacities of ASC-J9 and vehicle-treated SBMA mice by mating one male mouse with two B6 female mice for 1 week checking female mice for vaginal plugs each morning and recording litter sizes on delivery after four successive matings.

Histology and immunohistochemistry. We fixed tissues by 4% paraformaldehyde and embedded them in paraffin. For general histologic inspection, we treated tissue sections with H&E or NADH, and then used an ABC kit (Vector Laboratories) to detect AR immunostaining by an N20 antibody to AR. We performed the assessment of cells with intranuclear aggregated AR-polyQ in the ventral horn of the spinal cord as described previously[36,37]. We expressed the populations of AR-positive cells as the number per square millimeter. We counted AR-positive cells in randomly selected areas from more than 500 muscle fibers and expressed AR-positive cells as the number per 100 muscle fibers.

Quantitative real time RT-PCR. We harvested L5 spinal cords of mice treated with vehicle or ASC-J9 (50 mg/kg every 48 h), extracted total RNA using TRIZOL and reverse transcribed. We subjected 1 μg of total RNA to reverse transcription using Superscript II (Invitrogen), with the primer probe sequences and PCR conditions for VEGF164 as described previously[24]. We performed amplification, detection, and data analysis using a Bio-Rad iCycler system.

ELISA. We obtained total protein lysates by homogenizing tissues in an extraction buffer as described previously[24]. After centrifugation, we analyzed the amount of VEGF protein in the supernatant using ELISA kit (R&D Systems).

Statistical analysis. We analyzed the results by unpaired *t*-tests and log-rank tests for survival rate using Sigmaplot software. *P*-values less than 0.05 were considered to be statistically significant.

Note: Supplementary information is available on the Nature Medicine website.

ACKNOWLEDGMENTS

We thank K. Wolf for help in editing the manuscript. This work was supported by US National Institutes of Health grant DK067686 and the George Whipple Professorship Endowment.

COMPETING INTERESTS STATEMENT

The authors declare competing financial interests (see the *Nature Medicine* website for details).

Published online at http://www.nature.com/naturemedicine
Reprints and permissions information is available online at http://npg.nature.com/reprintsandpermissions

1. Kennedy, W.R., Alter, M. & Sung, J.H. Progressive proximal spinal and bulbar muscular atrophy of late onset: a sex-linked recessive trait. *Neurology* **50**, 583–593 (1998).
2. La Spada, A.R., Wilson, E.M., Lubahn, D.B., Harding, A.E. & Fischbeck, K.H. Androgen receptor gene mutations in X-linked spinal and bulbar muscular atrophy. *Nature* **352**, 77–79 (1991).
3. Ringel, S.P., Lava, N.S., Treihaft, M.M., Lubs, M.L. & Lubs, H.A. Late-onset X-linked recessive spinal and bulbar muscular atrophy. *Muscle Nerve* **1**, 297–307 (1978).
4. Sobue, G. *et al.* X-linked recessive bulbospinal neuronopathy. A clinicopathological study. *Brain* **112**, 209–232 (1989).
5. Katsuno, M. *et al.* Testosterone reduction prevents phenotypic expression in a transgenic mouse model of spinal and bulbar muscular atrophy. *Neuron* **35**, 843–854 (2002).
6. Li, M. *et al.* Nuclear inclusions of the androgen receptor protein in spinal and bulbar muscular atrophy. *Ann. Neurol.* **44**, 249–254 (1998).

7. Chang, C.S., Kokontis, J. & Liao, S.T. Molecular cloning of human and rat complementary DNA encoding androgen receptors. *Science* **240**, 324–326 (1988).
8. Heinlein, C.A. & Chang, C. Androgen receptor in prostate cancer. *Endocr. Rev.* **25**, 276–308 (2004).
9. Yeh, S. & Chang, C. Cloning and characterization of a specific coactivator, ARA70, for the androgen receptor in human prostate cells. *Proc. Natl. Acad. Sci. USA* **93**, 5517–5521 (1996).
10. Heinlein, C.A. & Chang, C. Androgen receptor (AR) coregulators: an overview. *Endocr. Rev.* **23**, 175–200 (2002).
11. McCampbell, A. & Fischbeck, K.H. Polyglutamine and CBP: fatal attraction? *Nat. Med.* **7**, 528–530 (2001).
12. Sherman, M.Y. & Goldberg, A.L. Cellular defenses against unfolded proteins: a cell biologist thinks about neurodegenerative diseases. *Neuron* **29**, 15–32 (2001).
13. Ross, C.A. Polyglutamine pathogenesis: emergence of unifying mechanisms for Huntington's disease and related disorders. *Neuron* **35**, 819–822 (2002).
14. Merry, D.E., Kobayashi, Y., Bailey, C.K., Taye, A.A. & Fischbeck, K.H. Cleavage, aggregation and toxicity of the expanded androgen receptor in spinal and bulbar muscular atrophy. *Hum. Mol. Genet.* **7**, 693–701 (1998).
15. Tarlac, V. & Storey, E. Role of proteolysis in polyglutamine disorders. *J. Neurosci. Res.* **74**, 406–416 (2003).
16. Mandrusiak, L.M. *et al.* Transglutaminase potentiates ligand-dependent proteasome dysfunction induced by polyglutamine-expanded androgen receptor. *Hum. Mol. Genet.* **12**, 1497–1506 (2003).
17. Beauchemin, A.M. *et al.* Cytochrome c oxidase subunit Vb interacts with human androgen receptor: a potential mechanism for neurotoxicity in spinobulbar muscular atrophy. *Brain Res. Bull.* **56**, 285–297 (2001).
18. Katsuno, M. & Sobue, G. Polyglutamine diminishes VEGF; passage to motor neuron death? *Neuron* **41**, 677–679 (2004).
19. Katsuno, M. *et al.* Leuprorelin rescues polyglutamine-dependent phenotypes in a transgenic mouse model of spinal and bulbar muscular atrophy. *Nat. Med.* **9**, 768–773 (2003).
20. Minamiyama, M. *et al.* Sodium butyrate ameliorates phenotypic expression in a transgenic mouse model of spinal and bulbar muscular atrophy. *Hum. Mol. Genet.* **13**, 1183–1192 (2004).
21. Chevalier-Larsen, E.S. *et al.* Castration restores function and neurofilament alterations of aged symptomatic males in a transgenic mouse model of spinal and bulbar muscular atrophy. *J. Neurosci.* **24**, 4778–4786 (2004).
22. Ohtsu, H. *et al.* Antitumor agents. 217. Curcumin analogues as novel androgen receptor antagonists with potential as anti-prostate cancer agents. *J. Med. Chem.* **45**, 5037–5042 (2002).
23. Walcott, J.L. & Merry, D.E. Ligand promotes intranuclear inclusions in a novel cell model of spinal and bulbar muscular atrophy. *J. Biol. Chem.* **277**, 50855–50859 (2002).
24. Sopher, B.L. *et al.* Androgen receptor YAC transgenic mice recapitulate SBMA motor neuronopathy and implicate VEGF164 in the motor neuron degeneration. *Neuron* **41**, 687–699 (2004).
25. Waza, M. *et al.* 17-AAG, an Hsp90 inhibitor, ameliorates polyglutamine-mediated motor neuron degeneration. *Nat. Med.* **11**, 1088–1095 (2005).
26. Goetz, M.P., Toft, D.O., Ames, M.M. & Erlichman, C. The Hsp90 chaperone complex as a novel target for cancer therapy. *Ann. Oncol.* **14**, 1169–1176 (2003).
27. Solit, D.B. *et al.* 17-Allylamino-17-demethoxygeldanamycin induces the degradation of androgen receptor and HER-2/neu and inhibits the growth of prostate cancer xenografts. *Clin. Cancer Res.* **8**, 986–993 (2002).
28. Barent, R.L. *et al.* Analysis of FKBP51/FKBP52 chimeras and mutants for Hsp90 binding and association with progesterone receptor complexes. *Mol. Endocrinol.* **12**, 342–354 (1998).
29. Smith, D.F. *et al.* Progesterone receptor structure and function altered by geldanamycin, an hsp90-binding agent. *Mol. Cell. Biol.* **15**, 6804–6812 (1995).
30. Hostein, I., Robertson, D., DiStefano, F., Workman, P. & Clarke, P.A. Inhibition of signal transduction by the Hsp90 inhibitor 17-allylamino-17-demethoxygeldanamycin results in cytostasis and apoptosis. *Cancer Res.* **61**, 4003–4009 (2001).
31. Banerji, U. *et al.* Phase I pharmacokinetic and pharmacodynamic study of 17-allylamino, 17-demethoxygeldanamycin in patients with advanced malignancies. *J. Clin. Oncol.* **23**, 4152–4161 (2005).
32. Price, J.T. *et al.* The heat shock protein 90 inhibitor, 17-allylamino-17-demethoxygeldanamycin, enhances osteoclast formation and potentiates bone metastasis of a human breast cancer cell line. *Cancer Res.* **65**, 4929–4938 (2005).
33. Thin, T.H. *et al.* Mutations in the helix 3 region of the androgen receptor abrogate ARA70 promotion of 17beta-estradiol-induced androgen receptor transactivation. *J. Biol. Chem.* **277**, 36499–36508 (2002).
34. Wang, L. *et al.* Suppression of androgen receptor-mediated transactivation and cell growth by the glycogen synthase kinase 3 beta in prostate cells. *J. Biol. Chem.* **279**, 32444–32452 (2004).
35. Garden, G.A. *et al.* Polyglutamine-expanded ataxin-7 promotes non-cell-autonomous purkinje cell degeneration and displays proteolytic cleavage in ataxic transgenic mice. *J. Neurosci.* **22**, 4897–4905 (2002).
36. Adachi, H. *et al.* Transgenic mice with an expanded CAG repeat controlled by the human AR promoter show polyglutamine nuclear inclusions and neuronal dysfunction without neuronal cell death. *Hum. Mol. Genet.* **10**, 1039–1048 (2001).
37. Terao, S. *et al.* Age-related changes in human spinal ventral horn cells with special reference to the loss of small neurons in the intermediate zone: a quantitative analysis. *Acta Neuropathol. (Berl.)* **92**, 109–114 (1996).

ELSEVIER

Neurobiology of Disease

www.elsevier.com/locate/ynbdi
Neurobiology of Disease 25 (2007) 331 – 341

Dorfin-CHIP chimeric proteins potently ubiquitylate and degrade familial ALS-related mutant SOD1 proteins and reduce their cellular toxicity

Shinsuke Ishigaki,[a,b] Jun-ichi Niwa,[a] Shin-ichi Yamada,[a] Miho Takahashi,[a] Takashi Ito,[a] Jun Sone,[a] Manabu Doyu,[a] Fumihiko Urano,[b,c] and Gen Sobue[a,*]

[a]*Department of Neurology, Nagoya University Graduate School of Medicine, Nagoya 466-8500, Japan*
[b]*Program in Gene Function and Expression, University of Massachusetts Medical School, Worcester, MA 01605, USA*
[c]*Program in Molecular Medicine, University of Massachusetts Medical School, Worcester, MA 01605, USA*

Received 19 May 2006; revised 8 September 2006; accepted 22 September 2006
Available online 6 December 2006

The ubiquitin–proteasome system (UPS) is involved in the pathogenetic mechanisms of neurodegenerative disorders, including amyotrophic lateral sclerosis (ALS). Dorfin is a ubiquitin ligase (E3) that degrades mutant SOD1 proteins, which are responsible for familial ALS. Although Dorfin has potential as an anti-ALS molecule, its life in cells is short. To improve its stability and enhance its E3 activity, we developed chimeric proteins containing the substrate-binding hydrophobic portion of Dorfin and the U-box domain of the carboxyl terminus of Hsc70-interacting protein (CHIP), which has strong E3 activity through the U-box domain. All the Dorfin-CHIP chimeric proteins were more stable in cells than was wild-type Dorfin ($Dorfin^{WT}$). One of the Dorfin-CHIP chimeric proteins, $Dorfin\text{-}CHIP^{L}$, ubiquitylated mutant SOD1 more effectively than did $Dorfin^{WT}$ and CHIP *in vivo*, and degraded mutant SOD1 protein more rapidly than $Dorfin^{WT}$ does. Furthermore, $Dorfin\text{-}CHIP^{L}$ rescued neuronal cells from mutant SOD1-associated toxicity and reduced the aggresome formation induced by mutant SOD1 more effectively than did $Dorfin^{WT}$.

Keywords: Dorfin; ALS; SOD1; CHIP; Neurodegeneration; Ubiquitin–proteasome system

Amyotrophic lateral sclerosis (ALS), one of the most common neurodegenerative disorders, is characterized by selective motor neuron degeneration in the spinal cord, brainstem, and cortex. About 10% of ALS cases are familial; of these, 10%–20% are caused by Cu/Zn superoxide dismutase (SOD1) gene mutations (Rosen et al., 1993; Cudkowicz et al., 1997). However, the precise mechanism that causes motor neuron death in ALS is still unknown, although many have been proposed: oxidative toxicity, glutamate receptor abnormality, ubiquitin proteasome dysfunction, inflammatory and cytokine activation, neurotrophic factor deficiency, mitochondrial damage, cytoskeletal abnormalities, and activation of the apoptosis pathway (Julien, 2001; Rowland and Shneider, 2001).

Misfolded protein accumulation, one probable cause of neurodegenerative disorders, including ALS, can cause the deterioration of various cellular functions, leading to neuronal cell death (Julien, 2001; Ciechanover and Brundin, 2003). Recent findings indicate that the ubiquitin–proteasome system (UPS), a cellular function that recognizes and catalyzes misfolded or impaired cellular proteins (Jungmann et al., 1993; Lee et al., 1996; Bercovich et al., 1997), is involved in the pathogenesis of various neurodegenerative diseases, among them ALS, Parkinson's disease (PD), Alzheimer's disease, polyglutamine disease, and prion disease (Alves-Rodrigues et al., 1998; Sherman and Goldberg, 2001; Ciechanover and Brundin, 2003). The ubiquitin ligase (E3), a key molecule for the UPS, can specifically recognize misfolded substrates and convey them to proteasomal degradation (Scheffner et al., 1995; Glickman and Ciechanover, 2002; Tanaka et al., 2004).

Dorfin, an E3 protein, contains an in-between-ring-finger (RING-IBR) domain at its N-terminus. The C-terminus of Dorfin can recognize mutant SOD1 proteins, which cause familial ALS (Niwa et al., 2001; Ishigaki et al., 2002b; Niwa et al., 2002). In cultured cells, Dorfin colocalized with aggresomes and ubiquitin-positive inclusions, which are pathological hallmarks of neurodegenerative diseases (Hishikawa et al., 2003; Ito et al., 2003). Dorfin also interacted with VCP/p97 in ubiquitin-positive inclusions in

Abbreviations: ALS, amyotrophic lateral sclerosis; CFTR, cystic fibrosis transmembrane conductance regulator; CHIP, carboxyl terminus of Hsc70-interacting protein; DMEM, Dulbecco's modified Eagle's medium; E3, ubiquitin ligase; FCS, fetal calf serum; IP, immunoprecipitation; LB, Lewy body; PD, Parkinson's disease; RING-IBR, in-between-ring-finger; SCF, Skp1-Cullin-F box complex; SDS-PAGE, sodium dodecyl sulfate-polyacrylamide gel electrophoresis; SOD1, Cu/Zn super oxide dismutase; UPS, ubiquitin–proteasome system.

* Corresponding author. Fax: +81 52 744 2384.
E-mail address: sobueg@med.nagoya-u.ac.jp (G. Sobue).
Available online on ScienceDirect (www.sciencedirect.com).

0969-9961/$ - see front matter © 2006 Elsevier Inc. All rights reserved.
doi:10.1016/j.nbd.2006.09.017

ALS and PD (Ishigaki et al., 2004). Moreover, formation of this complex was found to be necessary for the E3 activity of Dorfin against mutant SOD1. These findings suggest that Dorfin is involved in the quality-control system for the abnormal proteins that accumulate in the affected neurons in neurodegenerative disorders.

Dorfin degrades mutant SOD1s and attenuates mutant SOD1-associated toxicity in cultured cells (Niwa et al., 2002). However, in Dorfin/mutant SOD1 double transgenic mice, we found only a modest beneficial effect on mutant SOD1-induced survival and motor dysfunction (unpublished data). These findings, combined with the short half-life of Dorfin protein, led us to hypothesize that the limiting effect of the Dorfin transgene may be a consequence of autodegradation of Dorfin, since Dorfin can execute autoubiquitilation *in vivo* (Niwa et al., 2001).

Carboxyl terminus of Hsc70-interacting protein (CHIP) is also an E3 protein; it has a TPR domain in the N terminus and a U-box domain in the C terminus. The U-box domain of CHIP is responsible for its strong E3 activity, whereas the TPR domain recruits heat shock proteins harboring misfolded client proteins such as cystic fibrosis transmembrane conductance regulator (CFTR), denatured luciferase, and tau (Meacham et al., 2001; Murata et al., 2001, 2003; Hatakeyama et al., 2004; Shimura et al., 2004).

To prolong the protein lifetime of Dorfin and thereby obtain more potent ubiquitylation and degradation activity against mutant SOD1s than is provided by Dorfin or CHIP alone, we generated chimeric proteins containing the substrate-binding domain of Dorfin and the UPR domain of CHIP substitute for RING/IBR of Dorfin. We developed 12 candidate constructs that encode Dorfin-CHIP chimeric proteins and analyzed them for their E3 activities and degradation abilities against mutant SOD1 protein in cultured cells.

Experimental procedures

Plasmids and antibodies

We designed constructs expressing Dorfin-CHIP chimeric protein. In these constructs, different-length fragments of the C-terminus portion of Dorfin, including the hydrophobic substrate-binding domain (amino acids 333–838, 333–700, and 333–454) and the C-terminus UPR domain of CHIP with amino acids 128–303 or without amino acids 201–303, a charged region was fused in various combinations as shown in Fig. 2C. Briefly, Dorfin-CHIP$^{A, B, C, G, H,}$ and ^{I} had the C-terminus portion of Dorfin in their N-terminus and the U-box of CHIP in their C-terminus; Dorfin-CHIP$^{D, E, F, J, K}$, and ^{L} had the U-box of CHIP in their N-terminus and the C-terminus portion of Dorfin in their C-terminus.

We prepared a pCMV2/FLAG-Dorfin-CHIP chimeric vector (Dorfin-CHIP) by polymerase chain reaction (PCR) using the appropriate design of PCR primers with restriction sites (*Cla*I, *Kpn*I, and *XBa*I or *Eco*RI, *Cla*I, and *Kpn*I). The PCR products were digested and inserted into the *Cla*I–*Kpn*I site in pCMV2 vector (Sigma, St. Louis, MO). These vectors have been described previously: pFLAG-Dorfin^{WT} (Dorfin^{WT}), FLAG-Dorfin$^{C132S/C135S}$ (Dorfin$^{C132S/C135S}$), pFLAG-CHIP (CHIP), pFLAG-Mock (Mock), pcDNA3.1/Myc-SOD1^{WT} (SOD1^{WT}), pcDNA3.1/Myc-SOD1^{G93A} (SOD1^{G93A}), pcDNA3.1/Myc-SOD1^{G85R} (SOD1^{G85R}), pcDNA3.1/Myc-SOD1^{H46R} (SOD1^{H46R}), pcDNA3.1/Myc-SOD1^{G37R} (SOD1^{G37R}), pEGFP/SOD1^{WT} (SOD1^{WT}-GFP), and pEGFP/SOD1^{G85R} (SOD1^{G85R}-GFP) (Ishigaki et al., 2004). We used monoclonal anti-FLAG antibody (M2; Sigma), monoclonal anti-Myc antibody (9E10; Santa Cruz Biotechnology, Santa Cruz, CA), monoclonal anti-HA antibody (12CA5; Roche, Basel, Switzerland), and polyclonal anti-SOD1 (SOD-100; Stressgen, San Diego, CA).

Cell culture and transfection

We grew HEK293 cells and neuro2a (N2a) cells in Dulbecco's modified Eagle's medium (DMEM) containing 10% fetal calf serum (FCS), 5 U/ml penicillin, and 50 μg/ml streptomycin. At subconfluence, we transfected these cells with the indicated plasmids, using Effectene reagent (Qiagen, Valencia, CA) for HEK293 cells and Lipofectamine 2000 (Invitrogen, Carlsbad, CA) for N2a cells. After overnight posttransfection, we treated the cells with 1 μM MG132 (Z-Leu-Leu-Leu-al; Sigma) for 16 h to inhibit cellular proteasome activity. We analyzed the cells 24–48 h after transfection. To differentiate N2a cells, cells were treated for 48 h with 15 μM of retinoic acid in 2% serum medium.

Immunological analysis

At 24–48 h after transfection, we lysed cells (4×10^5 in 6-cm dishes) with 500 μl of lysis buffer consisting of 50 mM Tris–HCl, 150 mM NaCl, 1% Nonidet P-40, and 1 mM ethylenediaminetetraacetic acid (EDTA), as well as a protease inhibitor cocktail (Complete Mini, Roche). The lysate was then centrifuged at $10{,}000 \times g$ for 10 min at 4°C to remove debris. We used a 10% volume of the supernatants as the lysate for SDS-PAGE. When immunoprecipitated, the supernatants were precleared with protein A/G agarose (Santa-Cruz). A specific antibody, either anti-FLAG (M2) or anti-Myc (9E10), was then added. We incubated the immune complexes, first at 4°C with rotation and with protein A/G agarose (Roche) for 3 h, after which they were collected by centrifugation and washed four times with the lysis buffer. For protein analysis, immune complexes were dissociated by heating in SDS-PAGE sample buffer and loaded onto SDS-PAGE. We separated the samples by SDS-PAGE (15% gel or 5%–20% gradient gel) and transferred them onto polyvinylidene difluoride membranes. We then immunoblotted samples with specific antibodies.

Immunohistochemistry

We fixed differentiated N2a cells grown in plastic dishes in 4% paraformaldehyde in PBS for 15 min. The cells were then blocked for 30 min with 5% (vol/vol) normal goat serum in PBS, incubated overnight at 4°C with anti-FLAG antibody (M2), washed with PBS, and incubated for 30 min with Alexa 496 nm anti-mouse antibodies (Molecular Probes, Eugene, OR). We mounted the cells on slides and obtained images using a fluorescence microscope (IX71; Olympus, Tokyo, Japan) equipped with a cooled charge-coupled device camera (DP70; Olympus). Photographs were taken using DP Controller software (Olympus).

Analysis of protein stability

We assayed the stability of proteins by pulse-chase analysis using [^{35}S] followed by immunoprecipitation. Metabolic labeling was performed as described previously (Yoshida et al., 2003). Briefly, in the pulse-chase analysis of Dorfin proteins, HEK293 cells in 6-cm dishes were transiently transfected with 1 μg of

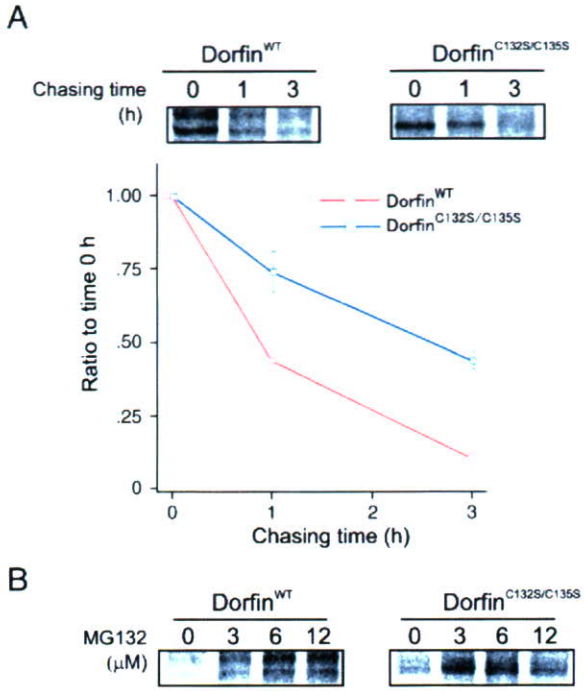

Fig. 1. Pulse-chase analysis of Dorfin^{WT} and Dorfin$^{C132S/C135S}$. (A) Dorfin^{WT} or Dorfin$^{C132S/C135S}$ was overexpressed in HEK293 cells. After overnight incubation, [^{35}S]-labeled Met/Cys pulse-chase analysis was performed. Cells were harvested and analyzed at 0, 1, or 3 h after labeling and immunoprecipitation by anti-FLAG antibody (upper panels). To determine serial changes in the amount of Dorfin^{WT} or Dorfin$^{C132S/C135S}$, four independent experiments were performed and the amounts of Dorfin^{WT} and Dorfin$^{C132S/C135S}$ were plotted. The differences between the amounts of Dorfin^{WT} and Dorfin$^{C132S/C135S}$ were significant at 1 h ($p<0.01$) and 3 h after labeling ($p<0.001$) (lower panels). Values are the means±SE, $n=4$. Statistics were done using an unpaired t-test. (B) Cells overexpressing Dorfin^{WT} or Dorfin$^{C132S/C135S}$ were treated with different concentrations of MG132 for 3 h after labeling.

FLAG-Dorfin^{WT} or FLAG-Dorfin$^{C132S/C135S}$. In pulse-chase experiments using SOD1^{G85R}, N2a cells in 6-cm dishes were transiently transfected with 1 μg of SOD1^{G85R}-Myc or SOD1^{G93A}-Myc and FLAG-Mock, FLAG-Dorfin, or FLAG-Dorfin-CHIP^{L}. FLAG-Mock was used as a negative control. After starving the cells for 60 min in methionine- and cysteine-free DMEM with 10% FCS, we labeled them for 60 min with 150 μCi/ml of Pro-Mix L-[^{35}S] *in vitro* cell-labeling mix (Amersham Biosciences). Cells were chased for different lengths of time at 37°C. In experiments with proteasomal inhibition, we added different amounts of MG132 in medium during the chase period. We performed immunoprecipitation using protein A/G agarose, mouse monoclonal anti-FLAG (M2), and anti-Myc (9E10). The intensity of the bands was quantified by ImageGauge software (Fuji Film, Tokyo, Japan).

MTS assay

We transfected N2a cells (5000 cells per well) in 96-well collagen-coated plates with 0.15 μg of SOD1^{G85R}-GFP and 0.05 μg of Dorfin, CHIP, Dorfin-CHIP^{L}, or pCMV2 vector (Mock) using Effecten reagent (Qiagen). Then we performed 3-(4,5-dimethylthiazol-2-yl)-5-(3-carboxymethoxyphenyl)-2-(4-sulfophenyl)-2*H*-tetrazolium inner salt (MTS) assays using Cell Titer 96 (Promega) at 48 h after incubation. This procedure has previously been described (Ishigaki et al., 2002a).

Aggregation assay

We transfected N2a cells in 6-cm dishes with 1.0 μg of SOD1^{G85R}-GFP and 1.0 μg of FLAG-Mock, FLAG-Dorfin, FLAG-CHIP, or FLAG-Dorfin-CHIP^{L}. After overnight incubation, we changed the medium to 2% FCS containing medium with 15 μM retinoic acid (RA) for differentiation. In the MG132 (+) group, 1 μM of MG132 was added after 24 h of differentiation stimuli. After 48 h of differentiation stimuli, we examined the cells in their living condition by fluorescence microscopy. The transfection ratio was equivalent (75%) among all groups. Visually observable macro aggregation-harboring cells were counted as "aggregation positive" cells (Fig. 7C). All cells were counted in fields selected at random from the four different quadrants of the culture dish. Counting was done by an investigator who was blind to the experimental condition.

Results

Dorfin degradation by the UPS in vivo

We analyzed the degradation speed of FLAG-Dorfin by the pulse-chase method using [^{35}S] labeling, finding that more than half of wild-type Dorfin (Dorfin^{WT}) was degraded within 1 h (Fig. 1A). This degradation was dose-dependently inhibited by MG132, a proteasome inhibitor (Fig. 1B). On the other hand, the RING mutant form of Dorfin (Dorfin$^{C132S/C135S}$), which lacks E3 activity (Ishigaki et al., 2004), degraded significantly more slowly than did Dorfin^{WT} (Fig. 1A and Table 1). As shown in Fig. 1A, Dorfin^{WT} showed two bands, whereas Dorfin$^{C132S/C135S}$ had a single band. This was also seen in our previous study (Ishigaki et al., 2004) and may represent posttranslational modification.

Construction of Dorfin-CHIP chimeric proteins

It is known that the C-terminus portion of Dorfin can bind to substrates such as mutant SOD1 proteins or Synphilin-1 (Niwa et al., 2002; Ito et al., 2003). We attempted to identify the domain of Dorfin that interacts with substrates. Although there was no obvious known motif in the C-terminus of Dorfin (amino acids 333–838), its first quarter contained rich hydrophobic amino acids (amino acids 333–454) (Fig. 2A). Immunoprecipitation analysis revealed that the hydrophobic region of Dorfin (amino acids 333–454) was able to bind to SOD1^{G85R}, indicating that this hydrophobic region is responsible for recruiting mutant SOD1 in Dorfin protein (Fig. 2B).

To establish more effective and more stable E3 ubiquitin ligase molecules that can recognize and degrade mutant SOD1s, we

Table 1
Serial changes in the amounts of Dorfin^{WT}, Dorfin$^{C132S/C135S}$, and Dorfin-CHIP^{L}

	0 h (%)	1 h (%)	3 h (%)
Dorfin^{WT}	100	43.7±7.0	10.3±4.4
Dorfin$^{C132S/C135S}$	100	73.9±13.8	43.7±1.9
Dorfin-CHIP^{L}	100	89.0±5.7	47.5±5.3

Values are the mean and SD of four independent experiments.

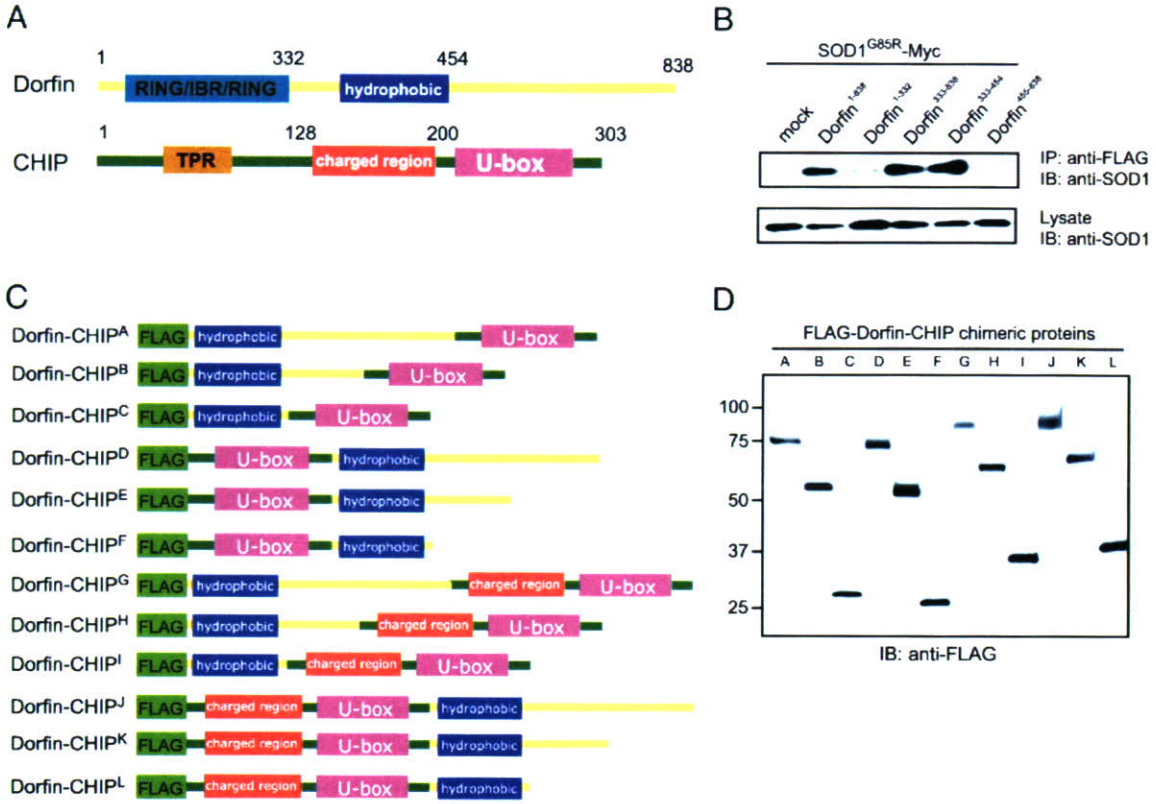

Fig. 2. Construction of Dorfin-CHIP chimeric proteins. (A) Dorfin has a RING/IBR domain in its N-terminus and a substrate-binding portion in the C-terminus. CHIP contains a TPR domain that binds to heat-shock proteins at the N-terminus; its C-terminal U-box domain has strong E3 ubiquitin ligase activity. (B) $SOD1^{G85R}$-Myc and FLAG-Dorfin derivatives were overexpressed in HEK 293 cells. Cell lysates were immunoprecipitated with anti-myc antibody. Immunoblotting showed that FLAG-Dorfin derivatives containing $Dorfin^{333-454}$ bound to $SOD1^{G85R}$-Myc, indicating that the hydrophobic region of Dorfin ($Dorfin^{333-454}$) is essential for interaction with mutant SOD1 *in vivo*. (C) Scheme of engineered Dorfin-CHIP chimeric proteins. Three different lengths of C-terminal Dorfin containing the hydrophobic region of Dorfin ($Dorfin^{333-454}$) and the U-box domain of CHIP with or without the charged region were fused. (D) Dorfin-CHIP chimeric proteins were overexpressed in HEK293 cells. Harvested cells were lysed and analyzed by immunoblotting using anti-FLAG antibody.

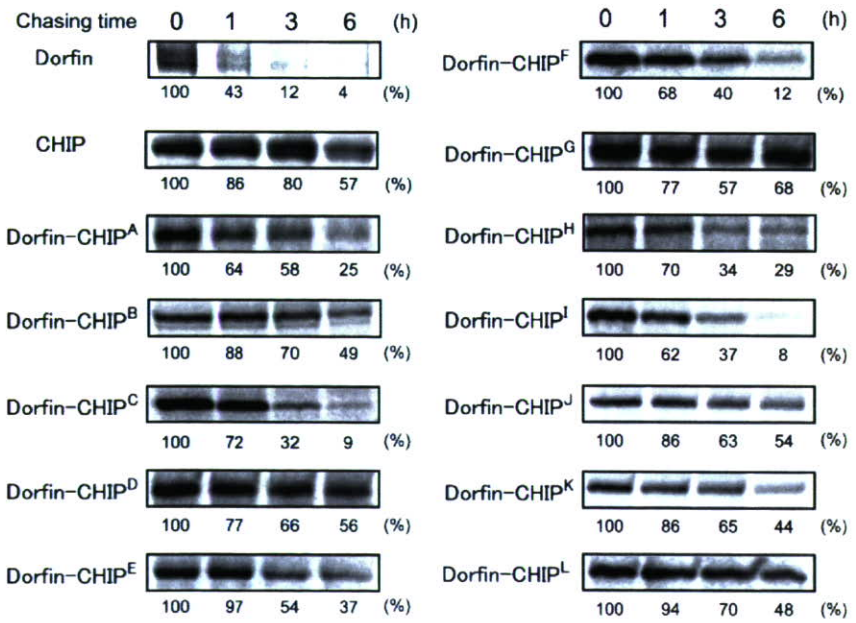

Fig. 3. The stability of Dorfin-CHIP chimeric proteins. Pulse-chase analysis using [^{35}S]-Met/Cys was performed. Dorfin, CHIP, and all the Dorfin-CHIP chimeric proteins were overexpressed in HEK293 cells and labeled with [^{35}S]-Met/Cys. Immunoprecipitation using anti-FLAG antibody and SOD-PAGE analysis revealed the degradation speed of FLAG-Dorfin-CHIP chimeric proteins. The amount of each Dorfin-CHIP chimeric protein was measured by quantifying the band using ImageGauge software.

designed Dorfin-CHIP chimeric proteins containing both the hydrophobic substrate-binding domain of Dorfin and the U-box domain of CHIP, which has strong E3 activity (Fig. 2C). We verified that all of the 12 candidate chimeric proteins were expressed in HEK293 cells (Fig. 2D).

Expression of Dorfin-CHIP chimeric proteins in cells

The half lives of all the Dorfin-CHIP chimeric proteins were more than 1 h. In some of these proteins, such as Dorfin-CHIP$^{D, G, J}$, and ^{L}, moderate amounts of protein still remained at 6 h after labeling, indicating that they were degraded much more slowly than was Dorfin^{WT} (Fig. 3). Repetitive experiments using Dorfin-CHIP^{L} yielded a significant difference between the amount of Dorfin^{WT} and Dorfin-CHIP^{L} at 1 h and 3 h (Table 1).

E3 activity of Dorfin-CHIP chimeric proteins against mutant SOD1

Immunoprecipitation analysis demonstrated that Dorfin and CHIP bound to mutant SOD1^{G85R} in equivalent amounts and that all of the Dorfin-CHIP chimeric proteins interacted with mutant SOD1^{G85R} *in vivo*. Dorfin-CHIP$^{A, D, E, F, J, K}$, and ^{L} bound to the same or greater amounts of SOD1^{G85R} than did Dorfin, whereas Dorfin-CHIP$^{B, C, G, H}$, and ^{I} did not (Fig. 4A, upper panel). None of the Dorfin-CHIP chimeric proteins bound to SOD1^{WT} *in vivo*

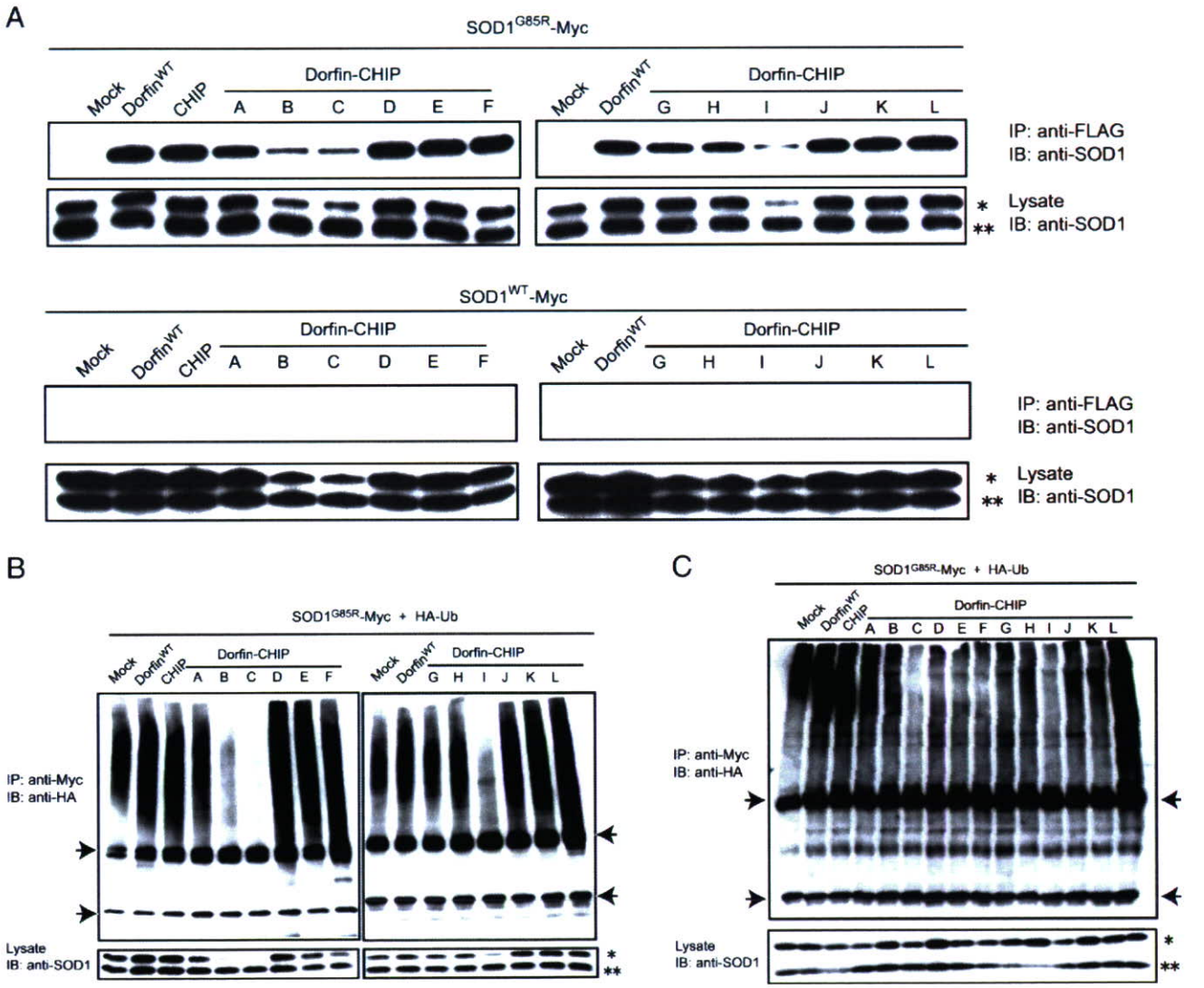

Fig. 4. The E3 activity of Dorfin-CHIP chimeric proteins on mutant SOD1 *in vivo*. (A) *In vivo* binding assay with both wild-type and mutant SOD1s. SOD1^{G85R}- or SOD1^{WT}-Myc and FLAG derivatives of Dorfin-CHIP chimeric proteins were coexpressed in HEK293 cells. Immunoprecipitation was done using anti-Myc antibody. Immunoblotting with anti-FLAG antibody revealed that all the Dorfin-CHIP chimeric proteins bound *in vivo* to SOD1^{G85R}-Myc but not to SOD1^{WT}-Myc. Single and double asterisks indicate overexpressed human SOD1s and mouse endogenous SOD1, respectively. (B) *In vivo* ubiquitylation assay in HEK293 cells. SOD1^{G85R}-Myc, HA-Ub, and FLAG derivatives of Dorfin-CHIP chimeric proteins were coexpressed in HEK293 cells. Immunoblotting with anti-HA antibody demonstrated the ubiquitylation level of SOD1^{G85R}-Myc by FLAG derivatives of Dorfin-CHIP chimeric proteins *in vivo*. Arrows indicate IgG light and heavy chains. Single and double asterisks indicate overexpressed SOD1 and mouse endogenous SOD1, respectively. (C) *In vivo* ubiquitylation assay in N2a cells. SOD1^{G85R}-Myc, HA-Ub, and FLAG derivatives of Dorfin-CHIP chimeric proteins were coexpressed in N2a cells. Arrows indicate IgG light and heavy chains. Single and double asterisks indicate overexpressed human SOD1s and mouse endogenous SOD1, respectively.

(Fig. 4A, lower panel). Some Dorfin-CHIP chimeric proteins, such as Dorfin-CHIP$^{B, C}$, and ^{I}, had lower amounts of both SOD1^{WT} and SOD1^{G85R} in the lysates. We performed quantitative RT-PCR using specific primers for SOD1-Myc, finding that coexpression of Dorfin-CHIP$^{B, C,}$ or ^{I} suppressed the mRNA expression of overexpressed SOD1 gene (Supplementary Fig. 1). Considering the possibility that these Dorfin-CHIP chimeric proteins might have unpredicted toxicity for cells by affecting gene transcription via unknown mechanisms, we excluded them from further analysis. Other Dorfin-CHIP proteins did not affect SOD1-Myc gene expression, which validated the comparison among IPs and ubiquitylated mutant SOD1 in Figs. 4A–C.

To assess the effectiveness of the E3 activity of Dorfin-CHIP chimeric proteins, we did an *in-vivo* ubiquitylation analysis by coexpression of SOD1^{G85R}-Myc, HA-Ub, and Dorfin-CHIP chimeric proteins in HEK293 cells. We found that Dorfin and CHIP enhanced the ubiquitylation of SOD1^{G85R} protein and that the ubiquitylation levels of these two E3 ligases were almost equivalent. Moreover, Dorfin-CHIP$^{D, E, F, J, K}$, and ^{L} ubiquitylated SOD1^{G85R} more effectively than did Dorfin or CHIP (Fig. 4B).

Performing the same *in-vivo* ubiquitylation assay using N2a cells, we observed that the levels of ubiquitylation of SOD1^{G85R} by Dorfin and CHIP were equivalent, as they were in HEK293 cells. Among Dorfin-CHIP chimeric proteins, only Dorfin-CHIP^{L}

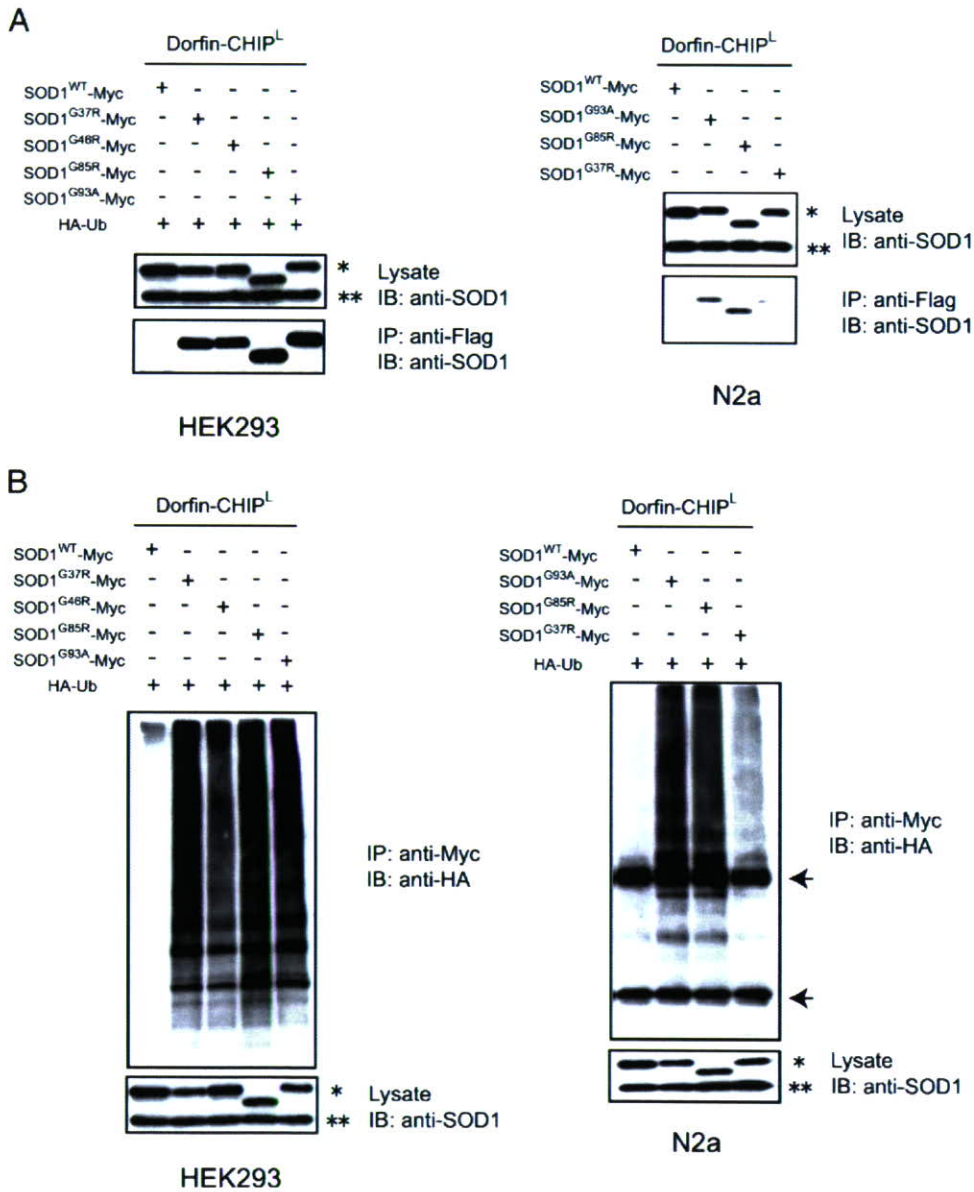

Fig. 5. Dorfin-CHIP^{L} specifically ubiquitylates mutant SOD1s *in vivo*. (A) *In vivo* binding assay with various mutant SOD1s. SOD1^{WT}-Myc, SOD1^{G93A}-Myc, SOD1^{G85R}-Myc, SOD1^{H46R}-Myc or SOD1^{G37R}-Myc, and FLAG-Dorfin-CHIP^{L} were coexpressed in HEK293 (left) and N2a cells (right). Immunoprecipitation was done using anti-Myc antibody. Immunoblotting with anti-FLAG antibody showed that both chimeric proteins specifically bound to mutant SOD1s *in vivo*. Single and double asterisks indicate overexpressed SOD1 and mouse endogenous SOD1, respectively. (B) *In vivo* ubiquitylation assay. SOD1^{WT}-Myc, SOD1^{G93A}-Myc, SOD1^{G85R}-Myc, SOD1^{H46R}-Myc or SOD1^{G37R}-Myc, as well as FLAG-Dorfin-CHIP^{L} and HA-Ub, was coexpressed in HEK293 (left) and N2a cells (right). Immunoblotting with anti-HA antibody showed the specific ubiquitylation of mutant SOD1-Myc by FLAG-Dorfin-CHIP^{L} *in vivo*. Arrows indicate IgG light and heavy chains. Single and double asterisks indicate overexpressed human SOD1s and mouse endogenous SOD1, respectively.

ubiquitylated SOD1^{G85R} more effectively than did Dorfin or CHIP, while Dorfin-CHIP$^{D, E, F, J}$, and ^{K} did not (Fig. 4C). Thus, Dorfin-CHIP^{L} was the most potent candidate of the chimeric proteins.

Ubiquitylation of mutant SOD1 by Dorfin-CHIP^{L}

Dorfin specifically ubiquitylated mutant SOD1 proteins, but not SOD1^{WT} protein (Niwa et al., 2002; Ishigaki et al., 2004). Similarly, Dorfin-CHIP^{L} interacted with SOD1^{G93A}, SOD1^{G85R}, SOD1^{H46R}, and SOD1^{G37R}, but not SOD1^{WT}, in HEK293 cells. This was confirmed in N2a cells (Fig. 5A). In both HEK293 and N2a cells, Dorfin-CHIP^{L} also ubiquitylated mutant SOD1 proteins but not SOD1^{WT} (Fig. 5B).

Degradation of mutant SOD1 by Dorfin-CHIP chimeric proteins

To assess the degradation activity of Dorfin-CHIP^{L} against mutant SOD1s, we performed the pulse-chase analysis on N2a

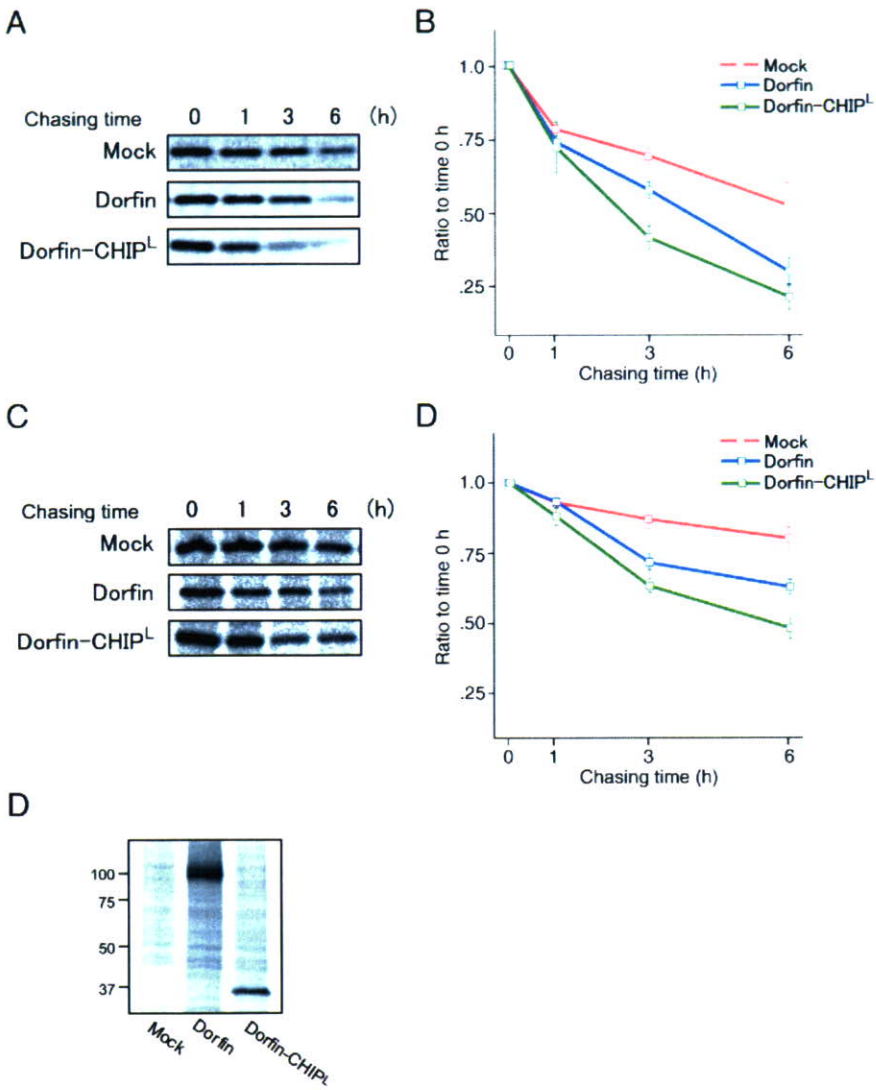

Fig. 6. Degradation of mutant SOD1 proteins with Dorfin-CHIP^{L}. (A) Pulse-chase analysis of SOD1^{G85R} with Dorfin-CHIP^{L}. N2a cells were coexpressed with SOD1^{G85R}-Myc and Mock, Dorfin, and Dorfin-CHIP^{L}. Pulse-chase experiments using [^{35}S]-Met/Cys were done. Immunoprecipitation using anti-Myc antibody and SOD-PAGE analysis revealed the degradation speed of SOD1^{G85R}-Myc. (B) Serial changes in the amount of SOD1^{G85R} coexpressed with Mock, Dorfin, or Dorfin-CHIP^{L}. Four independent experiments were performed and the amounts of SOD1^{G85R} were plotted. There were significant differences between Mock and Dorfin ($p<0.005$), Mock and Dorfin-CHIP^{L} ($p<0.005$), and Dorfin and Dorfin-CHIP^{L} ($p<0.05$) at 3 h, as well as between Mock and Dorfin ($p<0.05$), and Mock and Dorfin-CHIP^{L} ($p<0.05$) at 6 h after labeling. Values are the means±SE, $n=4$. Statistical analysis was done by one-way ANOVA. (C) Pulse-chase analysis of SOD1^{G93A} with Dorfin-CHIP^{L}. N2a cells were coexpressed with SOD1^{G93A}-Myc and Mock, Dorfin, and Dorfin-CHIP^{L} as in panel A. (D) Serial changes in the amount of SOD1^{G93A} coexpressed with Mock, Dorfin, or Dorfin-CHIP^{L}. Four independent experiments were performed and the amounts of SOD1^{G93A} were plotted. There were significant differences between Mock and Dorfin ($p<0.05$) and Mock and Dorfin-CHIP^{L} ($p<0.01$) at 3 h, as well as between Mock and Dorfin ($p<0.05$), Mock and Dorfin-CHIP^{L} ($p<0.01$), and Dorfin and Dorfin-CHIP^{L} ($p<0.05$) at 6 h after labeling. Values are the means±SE, $n=4$. Statistics were done by one-way ANOVA. (E) The equivalent protein expression levels of Dorfin and Dorfin-CHIP^{L}. Half of the volume of samples used in the pulse-chase analysis of panel C at 0 h was used for immunoprecipitation using anti-Flag M2 antibody. The following SOD-PAGE analysis revealed the amounts of Dorfin and Dorfin-CHIP^{L} in the experiment shown in panel C.

cells, using [^{35}S] labeled Met/Cys. The protein levels of SOD1^{G85R} and SOD1^{G93A} declined more rapidly with Dorfin coexpression. Dorfin-CHIP^{L} remarkably declined in both SOD1^{G85R} and SOD1^{G93A} (Figs. 6A, C). Dorfin and Dorfin-CHIP^{L} had similar expression levels at 0 h of this experiment (Fig. 6E). As compared to Mock, Dorfin showed significant declines of both SOD1^{G85R} at 3 h ($p<0.001$) and 6 h ($p<0.05$) after labeling, as shown in a previous study (Niwa et al., 2002). Dorfin-CHIP^{L} also significantly accelerated the decline of SOD1^{G85R} at 3 h ($p<0.001$) and 6 h ($p<0.05$) after labeling again as compared to Mock. At 3 h after labeling, a significant difference between Dorfin-CHIP^{L} and Dorfin was present with respect to SOD1^{G85R} degradation ($p<0.05$). As compared to Dorfin, Dorfin-CHIP^{L} also tended toward accelerated SOD1^{G85R} degradation at 6 h after labeling (Fig. 6B). Similarly, Dorfin showed significant declines of SOD1^{G93A} at 3 h ($p<0.05$) and 6 h ($p<0.05$) after labeling, and Dorfin-CHIP^{L} significantly accelerated the declines of SOD1^{G93A} at 3 h ($p<0.01$) and 6 h ($p<0.01$) after labeling as compared to Mock. A significant difference between Dorfin-CHIP^{L} and Dorfin was present at 6 h in SOD1^{G93A} degradation ($p<0.05$) (Fig. 6D).

Attenuation of the toxicity of mutant SOD1 and decrease in the formation of visible aggregations of mutant SOD1 in cultured neuronal culture cells

The ability of Dorfin-CHIP chimeric proteins to attenuate mutant SOD1-related toxicity was analyzed by MTS assay using N2a cells. The expression of SOD1^{G85R}, as compared to that of SOD1^{WT}, decreased the viability of cells. Overexpression of Dorfin reversed the toxic effect of SOD1^{G85R}, whereas overexpression of CHIP did not. Dorfin-CHIP^{L} had a significantly greater rescue effect on SOD1^{G85R}-related cell toxicity than did Dorfin (Fig. 7A). We also measured the cell viability of N2a cells overexpressing Mock, Dorfin, and Dorfin-CHIP^{L} with various amounts of constructs, and found no difference in toxicity among them (Supplementary Fig. 2).

A structure that Johnston et al. (1998) called aggresome is formed when the capacity of a cell to degrade misfolded proteins is exceeded. The accumulation of mutant SOD1 induces visible macroaggregation, which is considered to be 'aggresome' in N2a cells. We examined the subcellular localizations of Dorfin, CHIP, and Dorfin-CHIP^{L} by immunostaining N2a cells expressing SOD1^{G85R}-GFP. Dorfin was localized in aggresomes with substrate proteins, as in our previous studies. Dorfin-CHIP^{L} was also seen in aggresomes, whereas the staining of CHIP was diffusely observed in the cytosol (Fig. 7B). We counted these visible aggregations with or without MG132 treatment. Dorfin decreased the number of aggregation-containing cells, as has been reported (Niwa et al., 2002), but Dorfin-CHIP^{L} did so more effectively. These effects were inhibited by the treatment of MG132 (Fig. 7C).

Discussion

E3 proteins can specifically recognize and degrade accumulating aberrant proteins, which are deeply involved in the pathogenesis of neurodegenerative disorders, including ALS (Alves-Rodrigues et al., 1998; Sherman and Goldberg, 2001; Ciechanover and Brundin, 2003). For this reason, E3 proteins are candidate molecules for use in developing therapeutic technology for neurodegenerative diseases. Dorfin is the first E3 molecule that has been found specifically to ubiquitylate mutant SOD1 proteins as well as to attenuate mutant SOD-associated toxicity in cultured neuronal cells (Niwa et al., 2002).

NEDL1, a HECT type E3 ligase, has also been reported to be a mutant SOD1-specific E3 ligase and to interact with TRAPδ and dvl1 (Miyazaki et al., 2004). It has also been reported that ubiquitylation of mutant SOD1-associated complex was enhanced by CHIP and Hsp70 *in vivo* (Urushitani et al., 2004). CHIP ubiquitylated Hsp70-holding SOD1 complexes and degraded mutant SOD1, but did not directly interact with mutant SOD1 (Urushitani et al., 2004). Among these E3 molecules, Dorfin seems to be the most potentially beneficial E3 protein for use in ALS therapy since it is the only one that has been demonstrated to reverse mutant SOD1-associated toxicity (Niwa et al., 2002). Furthermore, Dorfin has been localized in various ubiquitin-positive inclusions such as Lewy bodies (LB) in PD, as well as LB-like inclusions in sporadic ALS and glial cell bodies in multiple-system atrophy. These findings indicate that Dorfin may be involved in the pathogenesis of a broad spectrum of neurodegenerative disorders other than familial ALS (Hishikawa et al., 2003; Ito et al., 2003; Ishigaki et al., 2004).

The half-life of Dorfin^{WT} is, however, less than 1 h (Fig. 1, Table 1). The amount of Dorfin is increased in the presence of MG132, a proteasome inhibitor, indicating that Dorfin is immediately degraded in the UPS. Since the nonfunctional RING mutant form of Dorfin, Dorfin$^{C132S/C135S}$, degraded more slowly than did Dorfin^{WT}, Dorfin seemed to be degraded by auto-ubiquitylation. The degradation of Dorfin$^{C132S/C135S}$ is also inhibited by MG132, suggesting that it is degraded by endogenous Dorfin or other E3s. This immediate degradation of Dorfin is a serious problem for its therapeutic application against neurodegenerative diseases.

Several reports have shown that engineered chimera E3s are able to degrade certain substrates with high efficiency. Protac, a chimeric protein-targeting molecule, was designed to target methionine aminopeptidase-2 to Skp1-Cullin-F box complex (SCF) ubiquitin ligase complex for ubiquitylation and degradation (Sakamoto et al.,

Fig. 7. Dorfin-CHIP chimeric proteins can attenuate toxicity induced by mutant SOD1 and decrease the formation of visible aggregation of mutant SOD1 in N2a cells. (A) N2a cells were grown in 96 collagen-coated wells (5000 cells per well) and transfected with 0.15 μg of SOD1^{WT} and 0.05 μg of Mock or 0.15 μg of SOD1^{G85R} and 0.05 μg of Mock, Dorfin, CHIP, or Dorfin-CHIP^{L}. After the medium was changed, MTS assays were done at 48 h of incubation. Viability was measured as the level of absorbance (490 nm). Values are the means±SE, $n=6$. Statistics were carried out by one-way ANOVA. There were significant differences between SOD1^{G85R}-expressing cells coexpressed with Mock and SOD1^{G85R}-expressing cells coexpressed with Dorfin ($p<0.001$), as well as between SOD1^{G85R}-expressing cells coexpressed with Dorfin and SOD1^{G85R}-expressing cells coexpressed with Dorfin-CHIP^{L} ($p<0.001$). (B) N2a cells were transiently expressed with SOD1^{G85R}-GFP and Mock, Dorfin, CHIP, or Dorfin-CHIP^{L}. Immunostaining with anti-FLAG antibody revealed that Dorfin, CHIP, and Dorfin-CHIP^{L} were localized with SOD1^{G85R}-GFP in macroaggresomes (arrows). Scale bar=20 μm (C) The visible macroaggregations in N2a cells expressing both SOD1^{G85R}-GFP and Mock, Dorfin, CHIP, or Dorfin-CHIP^{L} with or without MG132 treatment were counted and the ratio of cells with aggregations to those with GFP signals was calculated. Values are the means±SE, $n=4$. Statistics were done by one-way ANOVA. *$p<0.01$ denotes a significant difference between cells with Mock and Dorfin or Dorfin-CHIP^{L}. **$p<0.05$ denotes a significant difference between cells with Dorfin and Dorfin-CHIP^{L}.

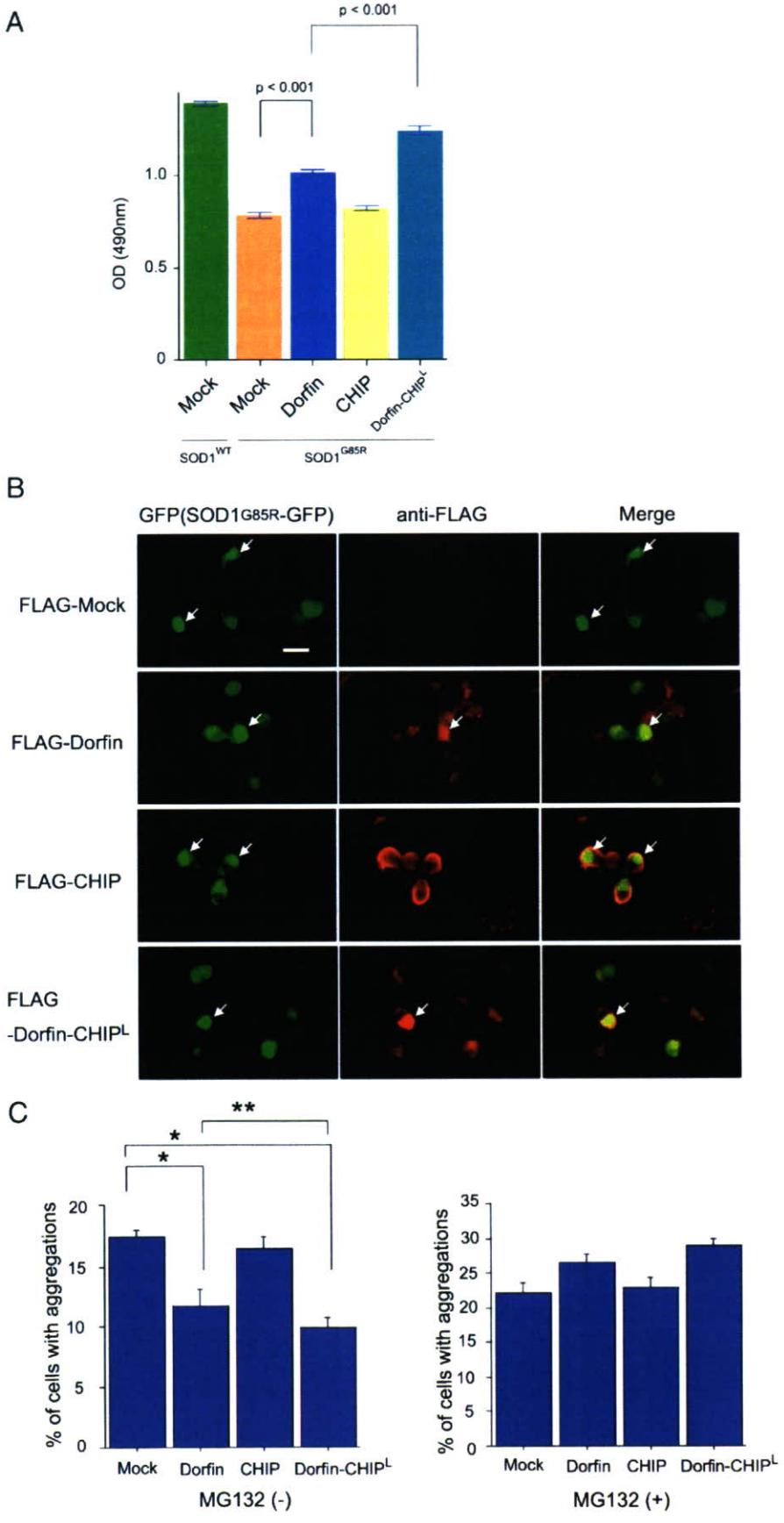
A
p < 0.001
p < 0.001
OD (490nm)
1.0
0.5
0
Mock
Mock
Dorfin
CHIP
Dorfin-CHIP^L
SOD1^WT
SOD1^G85R
B
GFP(SOD1G85R-GFP)
anti-FLAG
Merge
FLAG-Mock
FLAG-Dorfin
FLAG-CHIP
FLAG
-Dorfin-CHIP^L
C
**
*
*
% of cells with aggregations
20
15
10
5
0
Mock
Dorfin
CHIP
Dorfin-CHIP^L
MG132 (-)
35
30
25
20
15
10
5
0
Mock
Dorfin
CHIP
Dorfin-CHIP^L
MG132 (+)

2001, 2003). Oyake et al. (2002) developed double RING ubiquitin ligases containing the RING finger domains of both BRCA and BARD1 linked to a substrate recognition site PCNA. Recently, Hatakeyama et al. developed a fusion protein composed of Max, which forms a heterodimer with c-Myc, and the U-box of CHIP. This fusion protein physically interacted with c-Myc and promoted the ubiquitylation of c-Myc. It also reduced the stability of c-Myc, resulting in the suppression of transcriptional activity dependent on c-Myc and the inhibition of tumorogenesis (Hatakeyama et al., 2005). This indicated that the U-box portion of CHIP is able to add an effective E3 function to a U-box-containing client protein.

We postulated that engineered forms of Dorfin could be stable and still function as specific E3s for mutant SOD1s. Dorfin has a RING/IBR domain in the N-terminal portion (amino acids 1-332), but has no obvious motif in the rest of the C-terminus (amino acids 333–838). In this study, we have demonstrated that the hydrophobic domain of Dorfin (amino acids 333–454) is both necessary and sufficient for substrate recruiting (Fig. 2B). In our engineered proteins, the RING/IBR motif of N-terminal Dorfin was replaced by the UPR domain of CHIP, which had strong E3 activity (Murata et al., 2001). Some of the engineered Dorfin-chimeric proteins, such as Dorfin-CHIP$^{D, G, J}$, and ^{L}, were degraded *in vivo* far more slowly than was wild-type Dorfin, indicating that they were capable of being stably presented *in vivo* (Fig. 3). However, Dorfin-CHIP^{G} failed to show strong ubiquitylation activity against SOD1^{G85R} in HEK293 cells. Since Dorfin-CHIP$^{D, J}$, and ^{L} were able to bind to SOD1^{G85R} more strongly than did Dorfin-CHIP^{G}, the binding activity was more important for the E3 activity than for the protein stability.

We next showed that although all of the Dorfin-CHIP chimeric proteins bound to mutant SOD1 *in vivo*, some of them, such as Dorfin-CHIP$^{B, C}$, and ^{I}, bound less than others (Fig. 4A). In HEK293 cells, Dorfin-CHIP$^{D, E, F, J, K}$, and ^{L} ubiquitylated SOD1^{G85R} more effectively than did Dorfin or CHIP; however, in N2a cells only Dorfin-CHIP^{L} had more effective E3 activity than did Dorfin or CHIP. This discrepancy may be due to differences between HEK 293 and N2a cells which could provide slight different environment for the E3 machinery. Therefore, Dorfin-CHIP^{L} was the most potent of the candidate chimeric proteins in degrading mutant SOD1 in the UPS in neuronal cells. We also showed that Dorfin-CHIP^{L} could specifically bind to and ubiquitylate mutant SOD1s but not SOD1^{WT} *in vivo*, as Dorfin had done (Niwa et al., 2002; Ishigaki et al., 2004) (Fig. 5). This observation confirmed that the hydrophobic domain of Dorfin (amino acids 333–454) is responsible for mutant SOD1 recruiting.

Pulse-chase analysis using N2a cells showed that Dorfin-CHIP^{L} degraded SOD1^{G85R} and SOD1^{G93A} more effectively than did Dorfin (Fig. 6). This is compatible with the finding that Dorfin-CHIP^{L} had a greater effect than Dorfin did on the ubiquitylation against mutant SOD1. The cycloheximide assay verified that the degradation ability of Dorfin-CHIP^{L} against SOD1^{G85R} was stronger than that of Dorfin or CHIP in HEK293 cells (data not shown).

Dorfin-CHIP^{L} also reversed SOD1^{G85R}-associated toxicity in N2a cells more effectively than did Dorfin (Fig. 7). This therapeutic effect of Dorfin-CHIP^{L} was expected from its strong E3 activity and degradation ability against SOD1^{G85R}. Visible protein aggregations have been considered to be hallmarks of neurodegeneration. Increased understanding of the pathway involved in protein aggregation may demonstrate that visible macroaggregates represent the end-stage of a molecular cascade of steps rather than a direct toxic insult (Ross and Poirier, 2004). Two facts that Dorfin-CHIP^{L} decreased aggregation formation of SOD1^{G85R} and that this effect was inhibited by a proteasome inhibitor should reflect the ability of Dorfin-CHIP^{L} to degrade mutant SOD1 in the UPS of cells.

Based on our present observations, Dorfin-CHIP^{L}, an engineered chimeric molecule with the hydrophobic substrate-binding domain of Dorfin and the U-box domain of CHIP, had stronger E3 activity against mutant SOD1 than did Dorfin or CHIP. Indeed, it not only degraded mutant SOD1 more effectively than did Dorfin or CHIP but, as compared to Dorfin, produced marked attenuation of mutant SOD1-associated toxicity in N2a cells. This protective effect of Dorfin-CHIP^{L} against mutant SOD1 has potential applications to gene therapy for mutant SOD1 transgenic mice because this protein has a long enough life to allow the constant removal of mutant SOD1 from neurons. Since Dorfin was originally identified as a sporadic ALS-associated molecule (Ishigaki et al., 2002b) and is located in the ubiquitin-positive inclusions of various neurodegenerative diseases (Hishikawa et al., 2003), this molecule is an appropriate candidate for future use in gene therapy not only for familial ALS, but also for sporadic ALS and other neurodegenerative disorders.

So far, most reports on engineered chimera E3s have targeted cancer-promoting proteins. Dorfin-CHIP chimeric proteins are the first chimera E3s to be intended for the treatment of neurodegenerative diseases. Since the accumulation of ubiquitylated proteins in neurons is a pathological hallmark of various neurodegenerative diseases, development of chimera E3s like Dorfin-CHIP^{L}, which can remove unnecessary proteins, is a new therapeutic concept. Further analysis, including transgenic overexpression and vector delivery of Dorfin-CHIP chimeric proteins using ALS animal models will increase our understanding of the potential utility of Dorfin-CHIP chimeric proteins as therapeutic tools.

Acknowledgments

We gratefully thank Dr. Shigetsugu Hatakeyama at Hokkaido University for his advice about the construction of Dorfin-CHIP chimeric proteins. This work was supported by the Nakabayashi Trust for ALS Research; a grant for Center of Excellence (COE) from the Ministry of Education, Culture, Sports, Science and Technology of Japan; and grants from the Ministry of Health, Welfare and Labor of Japan.

Appendix A. Supplementary data

Supplementary data associated with this article can be found, in the online version, at doi:10.1016/j.nbd.2006.09.017.

References

Alves-Rodrigues, A., Gregori, L., Figueiredo-Pereira, M.E., 1998. Ubiquitin, cellular inclusions and their role in neurodegeneration. Trends Neurosci. 21, 516–520.

Bercovich, B., Stancovski, I., Mayer, A., Blumenfeld, N., Laszlo, A., Schwartz, A.L., Ciechanover, A., 1997. Ubiquitin-dependent degradation of certain protein substrates in vitro requires the molecular chaperone Hsc70. J. Biol. Chem. 272, 9002–9010.

Ciechanover, A., Brundin, P., 2003. The ubiquitin proteasome system in

neurodegenerative diseases: sometimes the chicken, sometimes the egg. Neuron 40, 427–446.

Cudkowicz, M.E., McKenna-Yasek, D., Sapp, P.E., Chin, W., Geller, B., Hayden, D.L., Schoenfeld, D.A., Hosler, B.A., Horvitz, H.R., Brown, R.H., 1997. Epidemiology of mutations in superoxide dismutase in amyotrophic lateral sclerosis. Ann. Neurol. 41, 210–221.

Glickman, M.H., Ciechanover, A., 2002. The ubiquitin–proteasome proteolytic pathway: destruction for the sake of construction. Physiol. Rev. 82, 373–428.

Hatakeyama, S., Matsumoto, M., Kamura, T., Murayama, M., Chui, D.H., Planel, E., Takahashi, R., Nakayama, K.I., Takashima, A., 2004. U-box protein carboxyl terminus of Hsc70-interacting protein (CHIP) mediates poly-ubiquitylation preferentially on four-repeat Tau and is involved in neurodegeneration of tauopathy. J. Neurochem. 91, 299–307.

Hatakeyama, S., Watanabe, M., Fujii, Y., Nakayama, K.I., 2005. Targeted destruction of c-Myc by an engineered ubiquitin ligase suppresses cell transformation and tumor formation. Cancer Res. 65, 7874–7879.

Hishikawa, N., Niwa, J., Doyu, M., Ito, T., Ishigaki, S., Hashizume, Y., Sobue, G., 2003. Dorfin localizes to the ubiquitylated inclusions in Parkinson's disease, dementia with Lewy bodies, multiple system atrophy, and amyotrophic lateral sclerosis. Am. J. Pathol. 163, 609–619.

Ishigaki, S., Liang, Y., Yamamoto, M., Niwa, J., Ando, Y., Yoshihara, T., Takeuchi, H., Doyu, M., Sobue, G., 2002a. X-Linked inhibitor of apoptosis protein is involved in mutant SOD1-mediated neuronal degeneration. J. Neurochem. 82, 576–584.

Ishigaki, S., Niwa, J., Ando, Y., Yoshihara, T., Sawada, K., Doyu, M., Yamamoto, M., Kato, K., Yotsumoto, Y., Sobue, G., 2002b. Differentially expressed genes in sporadic amyotrophic lateral sclerosis spinal cords—Screening by molecular indexing and subsequent cDNA microarray analysis. FEBS Lett. 531, 354–358.

Ishigaki, S., Hishikawa, N., Niwa, J., Iemura, S., Natsume, T., Hori, S., Kakizuka, A., Tanaka, K., Sobue, G., 2004. Physical and functional interaction between Dorfin and Valosin-containing protein that are colocalized in ubiquitylated inclusions in neurodegenerative disorders. J. Biol. Chem. 279, 51376–51385.

Ito, T., Niwa, J., Hishikawa, N., Ishigaki, S., Doyu, M., Sobue, G., 2003. Dorfin localizes to Lewy bodies and ubiquitylates synphilin-1. J. Biol. Chem. 278, 29106–29114.

Johnston, J.A., Ward, C.L., Kopito, R.R., 1998. Aggresomes: a cellular response to misfolded proteins. J. Cell Biol. 143, 1883–1898.

Julien, J.P., 2001. Amyotrophic lateral sclerosis. unfolding the toxicity of the misfolded. Cell 104, 581–591.

Jungmann, J., Reins, H.A., Schobert, C., Jentsch, S., 1993. Resistance to cadmium mediated by ubiquitin-dependent proteolysis. Nature 361, 369–371.

Lee, D.H., Sherman, M.Y., Goldberg, A.L., 1996. Involvement of the molecular chaperone Ydj1 in the ubiquitin-dependent degradation of short-lived and abnormal proteins in *Saccharomyces cerevisiae*. Mol. Cell. Biol. 16, 4773–4781.

Meacham, G.C., Patterson, C., Zhang, W., Younger, J.M., Cyr, D.M., 2001. The Hsc70 co-chaperone CHIP targets immature CFTR for proteasomal degradation. Nat. Cell Biol. 3, 100–105.

Miyazaki, K., Fujita, T., Ozaki, T., Kato, C., Kurose, Y., Sakamoto, M., Kato, S., Goto, T., Itoyama, Y., Aoki, M., Nakagawara, A., 2004. NEDL1, a novel ubiquitin–protein isopeptide ligase for dishevelled-1, targets mutant superoxide dismutase-1. J. Biol. Chem. 279, 11327–11335.

Murata, S., Minami, Y., Minami, M., Chiba, T., Tanaka, K., 2001. CHIP is a chaperone-dependent E3 ligase that ubiquitylates unfolded protein. EMBO Rep. 2, 1133–1138.

Murata, S., Chiba, T., Tanaka, K., 2003. CHIP: a quality-control E3 ligase collaborating with molecular chaperones. Int. J. Biochem. Cell Biol. 35, 572–578.

Niwa, J., Ishigaki, S., Doyu, M., Suzuki, T., Tanaka, K., Sobue, G., 2001. A novel centrosomal ring-finger protein, dorfin, mediates ubiquitin ligase activity. Biochem. Biophys. Res. Commun. 281, 706–713.

Niwa, J., Ishigaki, S., Hishikawa, N., Yamamoto, M., Doyu, M., Murata, S., Tanaka, K., Taniguchi, N., Sobue, G., 2002. Dorfin ubiquitylates mutant SOD1 and prevents mutant SOD1-mediated neurotoxicity. J. Biol. Chem. 277, 36793–36798.

Oyake, D., Nishikawa, H., Koizuka, I., Fukuda, M., Ohta, T., 2002. Targeted substrate degradation by an engineered double RING ubiquitin ligase. Biochem. Biophys. Res. Commun. 295, 370–375.

Rosen, D.R., Siddique, T., Patterson, D., Figlewicz, D.A., Sapp, P., Hentati, A., Donaldson, D., Goto, J., O'Regan, J.P., Deng, H.X., et al., 1993. Mutations in Cu/Zn superoxide dismutase gene are associated with familial amyotrophic lateral sclerosis. Nature 362, 59–62.

Ross, C.A., Poirier, M.A., 2004. Protein aggregation and neurodegenerative disease. Nat. Med. 10, S10–S17 (Suppl.).

Rowland, L.P., Shneider, N.A., 2001. Amyotrophic lateral sclerosis. N. Engl. J. Med. 344, 1688–1700.

Sakamoto, K.M., Kim, K.B., Kumagai, A., Mercurio, F., Crews, C.M., Deshaies, R.J., 2001. Protacs: chimeric molecules that target proteins to the Skp1-Cullin-F box complex for ubiquitination and degradation. Proc. Natl. Acad. Sci. U. S. A. 98, 8554–8559.

Sakamoto, K.M., Kim, K.B., Verma, R., Ransick, A., Stein, B., Crews, C.M., Deshaies, R.J., 2003. Development of Protacs to target cancer-promoting proteins for ubiquitination and degradation. Mol. Cell Proteomics 2, 1350–1358.

Scheffner, M., Nuber, U., Huibregtse, J.M., 1995. Protein ubiquitination involving an E1–E2–E3 enzyme ubiquitin thioester cascade. Nature 373, 81–83.

Sherman, M.Y., Goldberg, A.L., 2001. Cellular defenses against unfolded proteins: a cell biologist thinks about neurodegenerative diseases. Neuron 29, 15–32.

Shimura, H., Schwartz, D., Gygi, S.P., Kosik, K.S., 2004. CHIP–Hsc70 complex ubiquitinates phosphorylated tau and enhances cell survival. J. Biol. Chem. 279, 4869–4876.

Tanaka, K., Suzuki, T., Hattori, N., Mizuno, Y., 2004. Ubiquitin, proteasome and parkin. Biochim. Biophys. Acta 1695, 235–247.

Urushitani, M., Kurisu, J., Tateno, M., Hatakeyama, S., Nakayama, K., Kato, S., Takahashi, R., 2004. CHIP promotes proteasomal degradation of familial ALS-linked mutant SOD1 by ubiquitinating Hsp/Hsc70. J. Neurochem. 90, 231–244.

Yoshida, Y., Tokunaga, F., Chiba, T., Iwai, K., Tanaka, K., Tai, T., 2003. Fbs2 is a new member of the E3 ubiquitin ligase family that recognizes sugar chains. J. Biol. Chem. 278, 43877–43884.

Available online at www.sciencedirect.com
ScienceDirect
Behavioural Brain Research 185 (2007) 110–118
BEHAVIOURAL BRAIN RESEARCH
www.elsevier.com/locate/bbr

Research report

Alteration of behavioural phenotype in mice by targeted disruption of the progranulin gene

Yuko Kayasuga [a], Shuichi Chiba [a], Masatoshi Suzuki [a], Takefumi Kikusui [b], Takashi Matsuwaki [a], Keitaro Yamanouchi [a], Hayato Kotaki [c], Reiko Horai [c], Yoichiro Iwakura [c], Masugi Nishihara [a,*]

[a] *Department of Veterinary Physiology, Veterinary Medical Science, The University of Tokyo, 1-1-1 Yayoi, Bunkyo-ku, Tokyo 113-8657, Japan*
[b] *Department of Veterinary Ethology, Animal Resource Science, The University of Tokyo, Tokyo 113-8657, Japan*
[c] *Division of Cell Biology, Center for Experimental Medicine, Institute of Medical Science, The University of Tokyo, Tokyo 108-8639, Japan*

Received 30 March 2007; received in revised form 12 July 2007; accepted 15 July 2007
Available online 20 July 2007

Abstract

Sexual differentiation of the brain in rodents is achieved by estrogens, which are converted from androgens in the brain, during the perinatal period. We have identified the progranulin (PGRN) gene as one of the sex steroid-inducible genes that may be involved in masculinization of the rat brain. In the present study, we generated a line of mice with targeted disruption of the PGRN gene, and investigated male sexual behaviour, aggression and anxiety. PGRN-deficient mice exhibited a decrease in ejaculation incidence, while the latency and frequency of both mount and intromission were unchanged. For the aggressive behaviour test, the resident–intruder paradigm was used, and PGRN-deficient mice exhibited enhanced aggressiveness. In wild-type mice, males exhibited lower levels of anxiety than females by the open field test, while male PGRN-deficient mice exhibited an elevated level of anxiety and sex difference in anxiety was not observed. In addition, mRNA expression of the serotonergic receptor 5-HT1A, which could be related to the inhibition of aggression and anxiety, was significantly reduced in the hippocampus of PGRN-deficient mice after aggressive encounters. On the other hand, deficiency of the PGRN gene did not affect serum testosterone concentrations. These results suggest that PGRN gene plays a role in establishing sexual dimorphic behaviours at least partially by modulating the brain serotonergic system.

Keywords: Aggression; Anxiety; Frontotemporal dementia; Gene targeting; Progranulin; Sexual behaviour; Sexual differentiation

1. Introduction

It is well established that the mammalian brain possesses sexually dimorphic structure, which is reflected by functional sexual differences in the control of specific types of behaviour and endocrine patterns [1]. In rodent species, such as rats and mice, sexual dimorphism of the brain is established during the perinatal period, which is known as the critical period for brain sexual differentiation. During this period, androgens secreted from the testis masculinize the brain in males, while the female brain is not exposed to androgens and thereby develops into the "default" female type. In the brain, androgens are converted to estrogens by aromatase and are then involved in the masculinization of the brain through the facilitation of transcription of various factors [32].

In an attempt to identify genes that are involved in sexual differentiation of the brain, we have isolated the progranulin (PGRN) gene as an androgen-inducible gene in neonatal rat hypothalamus [45]. The expression of PGRN mRNA in the hypothalamus of males is maintained at high levels throughout the critical period, yet abruptly declines in females after birth. As estrogens can induce PGRN gene expression in the hypothalamus [48], androgens probably induce PGRN gene expression after being converted to estrogens. We further observed that infusion of an antisense oligodeoxynucleotide for the PGRN gene into the neonatal male rat brain significantly suppressed male sexual behaviours after maturation [46], suggesting that the PGRN gene is indeed involved in the process of masculin-

* Corresponding author. Tel.: +81 3 5841 5386; fax: +81 3 5841 8017.
E-mail address: amnishi@mail.ecc.u-tokyo.ac.jp (M. Nishihara).

0166-4328/$ – see front matter © 2007 Elsevier B.V. All rights reserved.
doi:10.1016/j.bbr.2007.07.020

ization of the rat brain. Recently, we have also found that PGRN is involved in estrogen-induced neurogenesis in the adult rat hippocampus [11].

In the mouse, the PGRN gene spans approximately 6.3 kbp and contains 13 exons [3]. PGRN mRNA has been demonstrated in various tissues and organs including the reproductive organs, gastrointestinal tract, endocrinal organs and neural tissues [9,17]. Peptides of approximately 6 kDa called granulins [6,8] also known as epithelins [42] are derived from PGRN. Both PGRN and granulins have growth-modulating effects on many cell types in culture [7,42]. For example, PGRN mediates the mitogenic effect of estrogens on MCF-7 cells, a human breast cancer cell line [30], which supports the above-mentioned notion that transcription of the PGRN gene is induced by estrogens. In addition, it has been recently reported that mutations in PGRN cause tau-negative, ubiquitin-positive frontotemporal dementia (FTD) in humans [4,16], suggesting that PGRN is involved in neuronal survival.

To elucidate the physiological roles of PGRN/granulins *in vivo*, especially their roles in the brain, we generated mice lacking the PGRN gene in the present study. Here, we describe their phenotypes regarding sexually dimorphic behaviours, such as sexual behaviour, aggression and anxiety.

2. Materials and methods

2.1. Generation of mice lacking the PGRN gene

A PGRN genomic clone was isolated from the 129 SvJ mouse genomic library (Stratagene, La Jolla, CA). The targeting vector was constructed by replacing an internal 4.7 kb EcoRV–EcoRI fragment, encoding exons 2–13 of the PGRN gene, with a PGK-Neo-bpA cassette [43] and by ligating the diphtheria toxin A (DT-A) fragment [54] to the 5′ end of the vector (Fig. 1A). The neomycin resistance gene, under the control of the phosphoglycerate kinase (PGK) 1 promoter, was inserted as a positive selection marker and DT-A fragment DNA, under the polyoma enhancer/herpes simplex virus thymidine promoter (MC-1), was used as a negative selection mechanism for the screening of recombinant embryonic stem (ES) cells. The targeting vector, linearized by ApaI, was electroporated (250 V, 5 μF) into 10^7 E14.1 ES cells [22], which were then selected with 250 μg/ml G418 (Gibco BRL, Grand Island, NY) for 7 days, as previously described [2]. Homologous recombination was confirmed by Southern blot analysis, as described below. For the generation of chimeric mice, ES cells were aggregated with two (C57BL/6 × DBF_1)

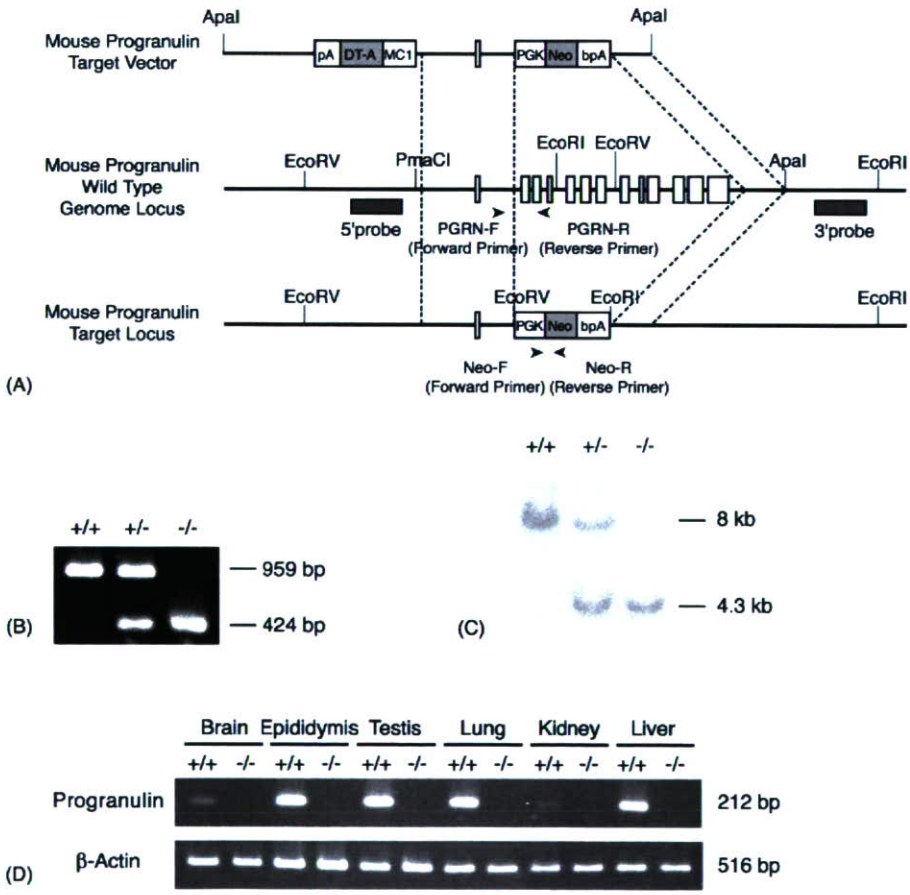

Fig. 1. Generation of mice with targeted disruption of the PGRN gene. (A) The targeting strategy for the mouse genomic PGRN locus. Construct of the targeting vector used to knockout the PGRN gene (top), the wild-type genome locus of mouse PGRN (middle) and the recombinated gene locus (bottom). In the mutant locus, the genomic region from exon 2 to exon 13 was replaced by the PGK-Neo-bpA cassette. The arrowheads indicate the location of the primers for PCR analysis and the grey boxes indicate the 5′ and 3′ probes for Southern blot analyses. Restriction enzyme sites used for linearization of the vector and Southern blot analyses are also indicated. (B) Bands detected in the PCR analysis of DNA from the tail of mice bred by $Grn^{+/-}$ intercrossing. The PCR products sized 959 bp correspond to the wild-type gene and the 424 bp bands correspond to the mutant gene. (C) Bands detected by Southern blot analysis using the 3′ probe following EcoRI digestion of genomic DNA from the tail of mice bred by $Grn^{+/-}$ intercrossing. The 8 kb fragment corresponds to the wild-type genome locus and the 4.3 kb bands correspond to the mutant genome locus. (D) PGRN gene expression in $Grn^{+/+}$ and $Grn^{-/-}$ mice. Total RNA was isolated from the brain, testis, epididymis, kidney, lung and liver of adult male $Grn^{+/+}$ and $Grn^{-/-}$ mice. The 212 bp bands correspond to PGRN and the 516 bp bands correspond to β-actin.

F_1 eight cell stage embryos, according to the method described previously [23].

Genotyping of offspring was carried out by PCR and Southern blot analysis with genomic DNA extracted from the tail of mice. The locus of PCR primers and probes, as well as the pattern diagrams of the targeting vector, are shown in Fig. 1A. The extraction of DNA for PCR and the PCR reactions were performed with a REDExtract-N-Amp Tissue PCR Kit (Sigma, Saint Louis, MO). The mutant gene was detected with the primers Neo-F (CCA ATA TGG GAT CGG CCA TTG AAC) and Neo-R (CGC TCG ATG CGA TGT TTC GCT TGG) and the wild-type (WT) gene with the primers PGRN-F (CAT GTG ACT GAT GAC TGT CC) and PGRN-R (GAG CAA GAC GCT TTT GCT TG). PCR reactions were carried out as follows: at 94 °C for 3 min for the initial denaturation, then 35 cycles at 94 °C for 30 s, 58 °C for 30 s and 72 °C for 30 s for amplification and 72 °C for 10 min for the final extension. Southern blot analysis was performed as previously reported [54]. Genomic DNA extracted from ES cell clones or mouse-tails were digested by EcoRV and EcoRI for the 5′ and 3′ probes flanking the targeting vector, respectively.

For RT-PCR, total RNA was isolated from the brain, testis, epididymis, kidney, lung and liver of adult wild-type ($Grn^{+/+}$) and PGRN-deficient ($Grn^{-/-}$) mice using TRIzol reagent (Gibco BRL, Grand Island, NY). First-strand cDNA was synthesized using Superscript II (Invitrogen, Carlsbad, CA) with oligo $d(T)_{16}$ primers (Roche, Mannheim, Germany). The forward and reverse primers used for PGRN were AGT TCG AAT GTC CTG ACT CCG CCA and AAG CCA CTG CCC TGT TGG TCC TTT, respectively, and those for β-actin (as positive control) were TCA GAA GGA CTC CTA TGT GG and GCA ACA TAG CAC AGC TTC TC, respectively. The PCR reactions were carried out in the following way: 10 min at 95 °C for initial denaturation, then 30 cycles at 94 °C for 45 s, 60 °C for 30 s and 72 °C for 1 min 45 s for amplification.

2.2. Animal care

All animal care and experiments were performed according to the guidelines for the Care and Use of Laboratory Animals, Graduate School of Agricultural and Life Sciences, the University of Tokyo. C57BL/6J and A/J mice were purchased from Sankyo Laboratory (Tokyo, Japan). Mice were group-housed in plastic cages and maintained on a 12 h light:12 h dark cycle (lights on at 07:00 h) at constant temperature (22–24 °C). Food (Lab MR Stock, Nihon Nousan Kougyou, Kanagawa, Japan) and water were available *ad libitum*. The line of the PGRN KO mouse was maintained by backcrossing $Grn^{+/-}$ males to C57BL/6J females. To breed the animals for the experiments, $Grn^{+/-}$ males were mated with $Grn^{+/-}$ females so that offspring with all genotypes were obtained in the same litter. In the experiment to compare litter size, $Grn^{+/+}$ and $Grn^{-/-}$ males were mated with $Grn^{+/+}$ and $Grn^{-/-}$ females, respectively. Pups were weaned at 30 days of age and tail tissue sampled for genotyping. Some of the adult males (11 weeks old), which had not been used for any other experiments, were sacrificed by decapitation under ether anesthesia and blood samples collected. Serum was separated and stored at −80 °C until assayed for testosterone. Serum concentrations of testosterone were determined with a testosterone EIA kit (Cayman Chemical, Ann Arbor, MI).

2.3. Behavioural analyses

Male sexual behaviour, aggression and anxiety were investigated using the mice at the age of 7–11 weeks. For each behavioural experiment, separate groups of mice were used. In the male sexual behaviour test, each male was isolated 1 h before the test, and tested for 1 h with a sexually naive C57BL/6J female mouse. All the stimulus females were ovariectomized and subcutaneously injected with 20 μg 17β-estradiol (48 and 24 h before the test) and 500 μg progesterone (4 h before the test) to ensure high sexual receptivity. The behaviour was videotaped and the numbers and latencies of mount and intromission were recorded. The incidence of ejaculation (percentage of animals that ejaculated) was determined by the existence of vaginal plugs in the females after each test. Aggressive behaviours toward females were also recorded. An aggressive bout was defined as a continuous series of behavioural interactions including at least one aggressive behavioural act, i.e., biting, aggressive grooming and tail rattling. If the interval between the occurrences of two aggressive behavioural acts exceeded 3 s, the behavioural act was scored as two separate aggressive bouts. The tests were performed between 20:00 and 21:00 h, and repeated three times for each male at 4-day intervals.

For the aggressive behaviour test, the resident–intruder paradigm [35] was used. Each male was isolated 1 h before the test and tested in his home cage (as a resident) against a group-housed (6–8 mice per cage) male A/J intruder mouse, and the behaviour videotaped for up to 15 min. Latency to the first biting attack and the number of biting attacks during a 5 min period after the first attack were recorded. When mice did not show any biting behaviour for 10 min, the test was stopped and the latency regarded as 10 min. The tests were performed between 12:00 and 16:00 h, and repeated three times for each male at 3-day intervals. Each male encountered a novel intruder at every trial. To evaluate locomotor activity during the test, the duration of walking and the number of rearings was recorded for 5 min after the first attack in the first trial. When there was no biting, the latter 5 min of the 10-min period videotaped was used to evaluate locomotor activity.

To evaluate anxiety, the open field test was performed. The mice were moved to the experimental room more than 1 h before the start of the test. The open field was composed of 50 cm × 50 cm surrounded by 40-cm-high wooden walls painted white. The tests were performed between 13:00 and 17:00 h, and the area was cleaned between mice. Each mouse was introduced in the center of the square and its behaviour was recorded on videotape for 10 min. The duration when the mouse stayed in the peripheral zone (7.5 cm from the wall) or the center, and the distance traveled and incidence of rearings in either area, were analyzed using a computerized technique with ethovision 3.0 (Noldus, Wageningen, Netherlands).

2.4. Quantitative real-time PCR

Using different groups of mice from those used for behavioural tests mentioned above, 5-hydoroxytriptamine receptor 1A (5-HT1A) and 5-HT1B mRNA levels in the hippocampus were determined after aggressive encounters. Male mice of each genotype were isolated from their home cages 1 h before the encounter with male A/J intruder mice. The behaviour was observed for 15 min and whether the intruder was attacked or not was checked. The encounters were repeated three times for each male at 2- or 3-day intervals. Control mice were similarly isolated three times but did not encounter any intruders. Right after the third test, mice were sacrificed and total RNA was isolated from the hippocampus. RNA isolation and first-strand cDNA synthesis were done as described above. Then real-time PCR was performed using the cDNA as a template. PCR reactions were performed with QuantiTect SYBR Green PCR (Qiagen, Hilden, Germany) and a Light Cycler (Roche, Mannheim, Germany). The forward and reverse primers used for 5-HT1A were TCG CTC ACT TGG CTC ATT GGC TTT and TTC CAA CTT CTT GAC CGT CTT GCG, respectively, and those for 5-HT1B were GCT GGA CTG CTT TGT GAA CAC CGA and AAT GGA GGT GAC CGA GGA TGT GGA, respectively. The forward and reverse primers used for hypoxanthine phosphoribosyltransferase (HPRT; as an internal standard) were CTT GAG CAC ACA GAG GGC CAC AAT and AGT CCC AGC GTC GTG ATT AGC GAT, respectively. The PCR reactions were carried out in the following way for 5-HT1A and HPRT: 15 min at 95 °C for the initial denaturation, then 35 cycles at 95 °C for 30 s, 60 °C for 20 s and 72 °C for 20 s for amplification, and for 5-HT1B: 15 min at 95 °C for the initial denaturation, then 35 cycles at 95 °C for 15 s, 60 °C for 30 s and 72 °C for 20 s for amplification.

2.5. Statistical analyses

Except for the incidence of ejaculation, the data from the behavioural analyses, and 5-HT mRNA expression analyses were analyzed by repeated or non-repeated two-way analysis of variance (ANOVA) followed by post hoc comparison with Fisher's PLSD or Holm's test. The incidence of ejaculation data was analyzed by Fisher's exact probability test. The data from other experiments were analyzed by ANOVA followed by post hoc comparison with Fisher's PLSD test. The differences were considered statistically significant at $p < 0.05$.

3. Results

3.1. Generation of mice lacking the PGRN gene

We cloned the mouse PGRN gene and disrupted it in an ES cell line derived from the 129 SvJ mouse strain (Fig. 1A). Six targeted clones out of 547 were identified by Southern blot analysis and 3 of these (6D5, 18C4 and 19B2) had normal karyotypes and were used for the production of chimeric mice. The chimeric mice were mated with C57BL/6 females. One of the chimeras, 6D5-#6 was shown to be a germ line chimera and heterozygous offspring obtained from him were backcrossed to C57BL/6 females. Genotyping was carried out by PCR analysis with genomic DNA extracted from the tail. We detected bands of 959 bp using genomic DNA obtained from wild-type ($Grn^{+/+}$) mice as a template, a band of 424 bp from homozygous ($Grn^{-/-}$) mice and two bands of 959 and 424 bp from heterozygous ($Grn^{+/-}$) mice (Fig. 1B). To confirm the results of the PCR analysis, Southern blot analysis was also performed. Fig. 1C shows the result of Southern blot analysis using the 3′ probe

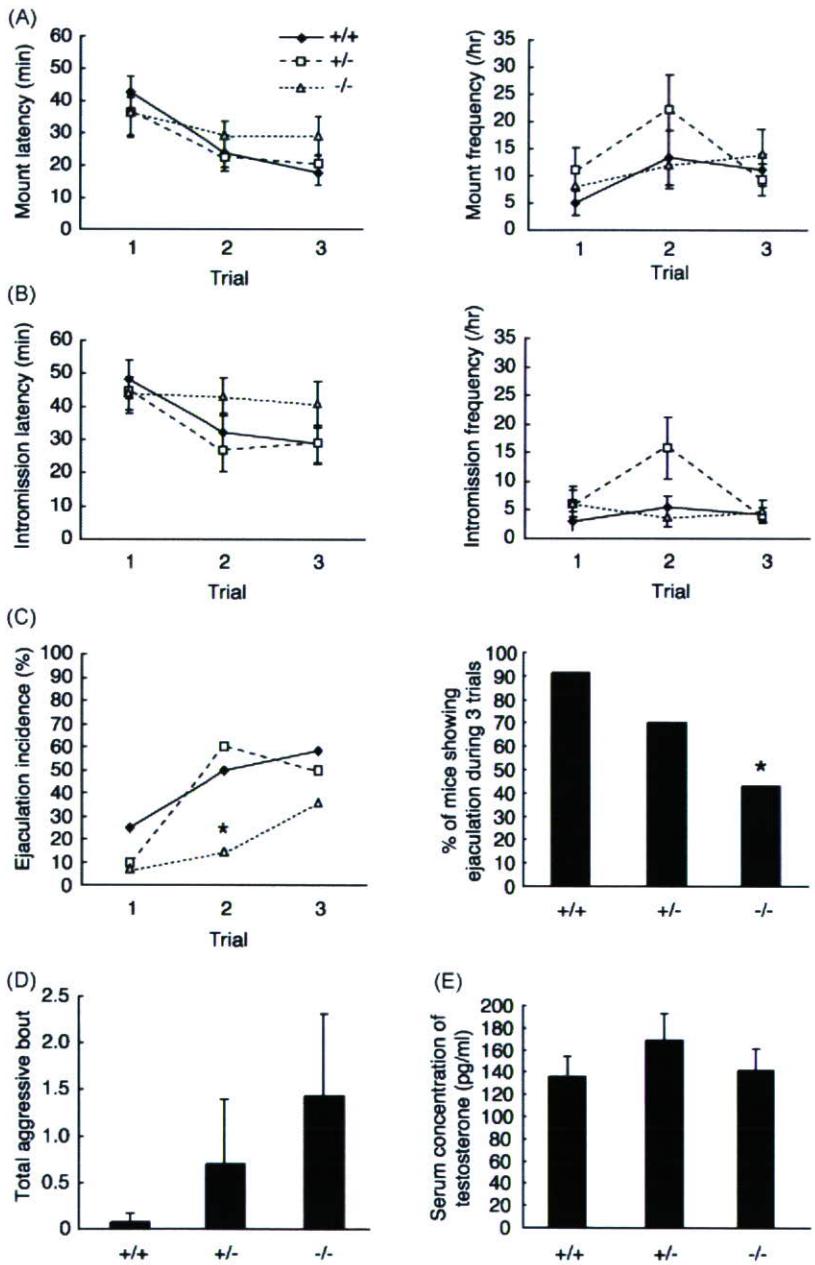

Fig. 2. Analysis of male sexual behaviour. Each male was tested for 1 h with a stimulus female and behaviour recorded. Tests were repeated three times for each male ($n = 12$ for $Grn^{+/+}$, $n = 10$ for $Grn^{+/-}$, $n = 14$ for $Grn^{-/-}$). (A) Latency (left) and frequency (right) of mount. Each symbol and vertical bar represents the mean and S.E.M., respectively. (B) Latency (left) and frequency (right) of intromission. Each symbol and vertical bar represents the mean and S.E.M., respectively. (C) Percentage of mice showing ejaculation in each trial (left) and over the three trials (right). The incidence of ejaculation was determined by the presence of vaginal plugs in females after the test. $^{*}p < 0.05$, Fisher's exact probability test, compared to $Grn^{+/+}$, $Grn^{+/-}$ (left) and to $Grn^{+/+}$ (right). (D) Total aggressive bouts toward stimulant females over the three trials. Each column and vertical bar represents the mean and S.E.M., respectively. (E) Serum testosterone concentrations in adult male mice. Each column and vertical bar represents the mean and S.E.M., respectively ($n = 4$ for each experimental group).